iScience

CellPress
OPEN ACCESS

Article

Single synapse glutamate imaging reveals multiple levels of release mode regulation in mammalian synapses

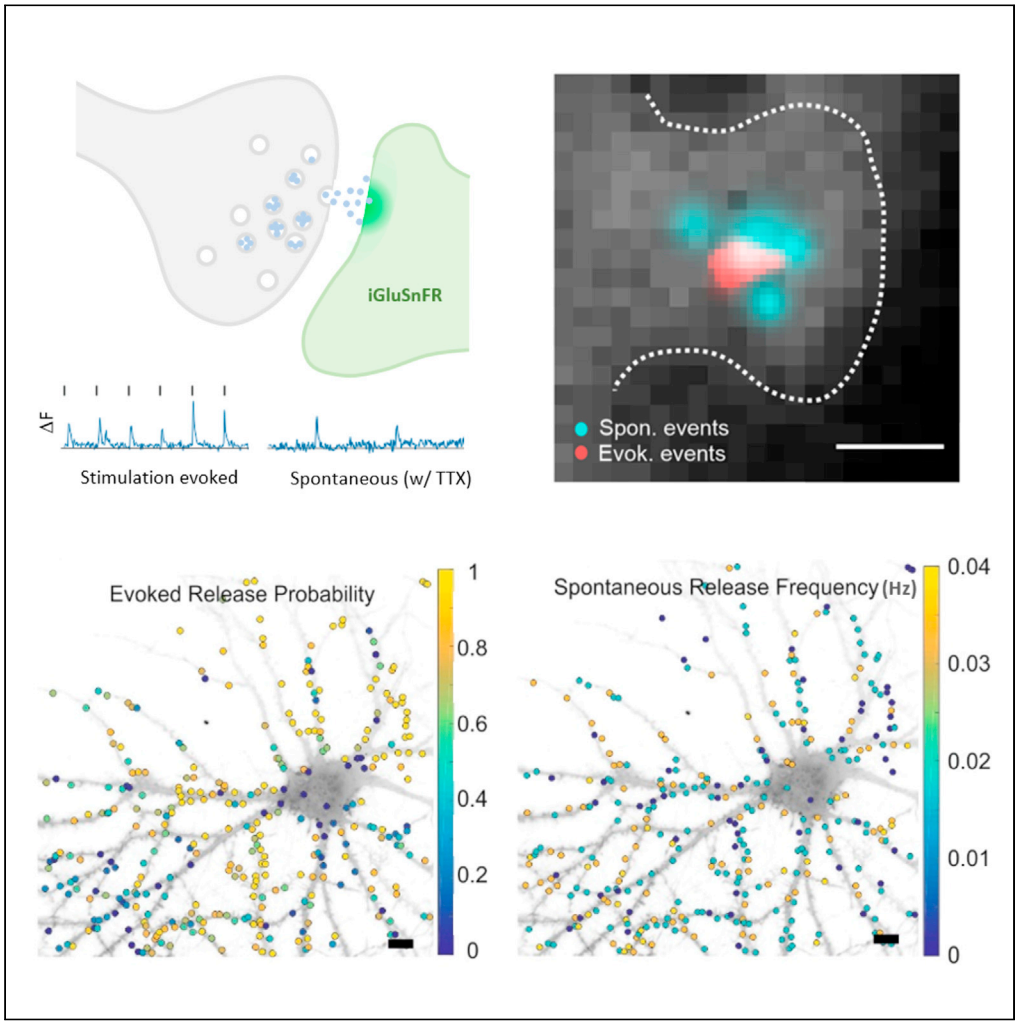

Zohreh Farsi, Marie Walde, Agnieszka E. Klementowicz, Foteini Paraskevopoulou, Andrew Woehler

andrew.woehler@mdc-berlin.de

Highlights

Glutamate imaging reveals high variability in release properties between synapses

Evoked and spontaneous synaptic release are regulated by distinct mechanisms

Spontaneous release is enhanced outside of evoked release region at the synapse

Distinct molecular ensembles contribute to spontaneous and evoked release

Farsi et al., iScience 24, 101909
January 22, 2021 © 2020 The Author(s).
https://doi.org/10.1016/j.isci.2020.101909

iScience

CellPress
OPEN ACCESS

Article

Single synapse glutamate imaging reveals multiple levels of release mode regulation in mammalian synapses

Zohreh Farsi,[1] Marie Walde,[1] Agnieszka E. Klementowicz,[1] Foteini Paraskevopoulou,[2] and Andrew Woehler[1,3,*]

Summary

Mammalian central synapses exhibit vast heterogeneity in signaling strength. To understand the extent of this diversity, how it is achieved, and its functional implications, characterization of a large number of individual synapses is required. Using glutamate imaging, we characterized the evoked release probability and spontaneous release frequency of over 24,000 individual synapses. We found striking variability and no correlation between action potential-evoked and spontaneous synaptic release strength, suggesting distinct regulatory mechanisms. Subpixel localization of individual evoked and spontaneous release events reveals tight spatial regulation of evoked release and enhanced spontaneous release outside of evoked release region. Using on-stage post hoc immune-labeling of vesicle-associated proteins, Ca^{2+}-sensing proteins, and soluble presynaptic proteins we were able to show that distinct molecular ensembles are associated with evoked and spontaneous modes of synaptic release.

Introduction

More than half a century ago, seminal work at the neuromuscular junction identified action potential (AP)-evoked and AP-independent spontaneous neurotransmission as two discrete modes of information transmission at chemical synapses (Fatt and Katz 1952). Upon stimulation of presynaptic terminals, the size of postsynaptic currents tended to occur at integer multiples of a quantal response. This quantal response corresponded with the amplitude of spontaneous "mini" postsynaptic potentials that occur in the absence of depolarization. Subsequent work identified synaptic vesicles (SVs) as the means of packaging and releasing these quanta of neurotransmitter during synaptic transmission. In the following decades a simplified model of the synaptic transmission was established in which, upon AP-induced calcium influx, synaptic vesicles fuse with a variable release probability at a variable number of discrete release sites within a presynaptic bouton. These two sources of variability have been suggested to be the key contributors to heterogeneity in AP-evoked postsynaptic potentials among synapses (Dobrunz and Stevens 1997).

Although there is consensus on many fundamental aspects of evoked synaptic transmission, the mechanisms and physiological relevance of spontaneous synaptic release remain contentious. Initially spontaneous release was believed to share the same presynaptic machinery as evoked release and merely be stochastic noise inherent in all synapses. Likewise, an abundance of work suggests that evoked and spontaneous release originate from the same pool of synaptic vesicles (Groemer and Klingauf 2007; Hua et al., 2010; Wilhelm et al., 2010). However, other work, employing similar methods has reached the opposite conclusion (Sara et al., 2005; Fredj and Burrone 2009). There is an emerging view that these two forms of release do result from differential presynaptic regulation (Groffen et al., 2010; Ramirez et al., 2012), can even target different postsynaptic receptors (Reese and Kavalali 2016), and play essential roles in homeostatic plasticity (Sutton and Schuman 2005). One key hindrance, preventing resolution of these inconsistencies, is the lack of adequate methods to directly study discrete release events at the synapse.

Our current mechanistic understanding of synaptic transmission is based primarily on decades of electrophysiological work at a limited number of large model synapses (Llinas et al., 1994; Geiger and Jonas 2000; von Gersdorff and Borst 2002). Interrogation of synaptic release from smaller "simple synapses" that constitute the majority of synapses in the central nervous system remains challenging (Malagon et al., 2016). Various fluorescent reporters allow for spatiotemporal discrimination of synaptic activity with optical

[1]Berlin Institute for Medical Systems Biology, Max Delbrück Center for Molecular Medicine, Berlin, 10115, Germany

[2]Institute of Neurophysiology, NeuroCure Cluster of Excellence, Charité-Universitätsmedizin, Berlin, 10115, Germany

[3]Lead contact

*Correspondence: andrew.woehler@mdc-berlin.de

https://doi.org/10.1016/j.isci.2020.101909

This is an open access article under the CC BY-NC-ND license (http://creativecommons.org/licenses/by-nc-nd/4.0/).

microscopy. FM dyes and pH-sensitive GFPs (pHluorins) have been used extensively to interrogate the synapse (Harata et al., 2001; Waters and Smith 2002; Leitz and Kavalali 2014). However, robust single vesicle response has been difficult to resolve above noise and variable probe copy number per vesicle convolutes quantal analysis. Calcium reporters that report on N-methyl-D-aspartate receptor (NMDAR)-mediated [Ca^{2+}] accumulation in individual spines have been shown to reliably report on single release events. However, the diffusion and accumulation of calcium limits accurate localization of release in space and time. Furthermore, both pre- and postsynaptic processes regulate the measured response amplitude (Melom et al., 2013; Peled et al., 2014). Recently, the development of fluorescent probes that directly report on glutamate concentration in the synaptic cleft (Okubo et al., 2010; Marvin et al., 2013) have shown great promise in providing the resolution required to "see" synaptic release.

In this work, we present a method for detecting and quantifying individual exocytotic events. We do this in a large field of view covering hundreds of synapses from dissociated hippocampal cultured neurons. We show that intensity-based glutamate-sensing fluorescent reporter (iGluSnFR) (Marvin et al., 2013) provides sufficient sensitivity to resolve quantal vesicle release. This resolution allows us to not only accurately characterize evoked release properties but also, importantly, reliably detect spontaneous events. We characterize evoked release probability as the fraction of stimuli for which response is detected and spontaneous fusion rates as the number of detected events per given time in the absence of stimuli. We measure these two properties at thousands of individual synapses and show that there is substantial variability among them but no correlation between them. We show that spontaneous release tends to occur over a larger area of the synapse. Utilizing on-stage post hoc immunostaining to measure the local abundance of synaptic constituents, we show that the inherent variability in synaptic properties and molecular composition can be used to predict the roles of synaptic proteins. Our results shed new light on the relationship between evoked and spontaneous release. Rather than the existence of master regulators of spontaneous release, this work suggests that a combination of different factors is preferentially associated with each release mode.

Results

Glutamate imaging provides a robust readout of discrete synaptic transmission events

To measure synaptic transmission at individual central synapses, we prepared primary hippocampal cultures from newborn (P0) rat brains and infected the cells with an adenovirus-associated construct to express iGluSnFR (Marvin et al., 2013). iGluSnFR uniformly distributed on the extracellular surface of cell body, dendritic arbor, and axonal projections of the neurons where it reports on extracellular glutamate concentration (Figures 1A and S1A, Videos S1 and S2). Upon low-frequency field stimulation, we observed small increases in fluorescence above background (Figure 1B, top panels), which were localized after high-pass filtering (magenta spots in Figure 1B). In addition to robust quantification of evoked release (Figure 1C, top trace, Figure S2), we were also able to resolve spontaneous glutamate release in the presence of 500 nM tetrodotoxin (TTX) at the dendritic spines (Figure 1C, bottom trace) and both release modes at axonal terminals (Figure S1C).

Quantal resolution and presence of multi-quantal release

To assess the quantal resolution of the sensor, we performed 5-min-long AP-evoked measurements of glutamate release during a train of electrical field stimuli at 0.5 Hz in the presence of 6-cyano-7-nitroquinoxaline-2,3-dione (CNQX) and 2-amino-5-phosphonovaleric acid (AP5), to block recurrent network activity. We then built histograms of stimulus-evoked fluorescence amplitudes from individual synapses. The resulting histograms often showed multiple peaks and fit well to a sum of Gaussian distributions (Akaike, 1973; McLachlan and Peel, 2000). The histograms shown in Figures 2A and 2B both have prominent peaks around zero, indicating frequent release failures. The second peak is centered about the unitary quantal amplitude. In some cases, clearly resolved peaks at integer multiples of the quantal amplitude were observed (Figures 2B and S3), providing an evidence of multiquantal release. These data clearly illustrate the quantal resolution of iGluSnFR, giving us the confidence to use this sensor to reliably identify all release events at small central synapse.

To compare the relative quantal amplitudes of evoked and spontaneous glutamate release at the same subset of synapses, we followed measurements during a 20 AP, 0.5-Hz train stimuli with a 5-min incubation in 500 nM TTX to block AP generation and then a 5-min measurement to sample spontaneous glutamate release. The amplitude and time course of evoked and spontaneous fluorescence changes in the same

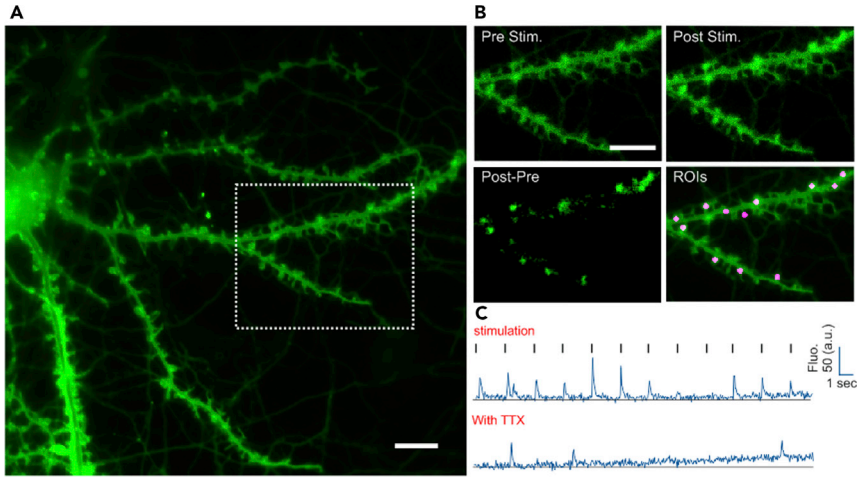

Figure 1. Glutamate imaging provides a robust signal of discrete synaptic transmission events

(A) When expressed in hippocampal neurons, iGluSnFR localizes to the outer leaflet of the plasma membrane.

(B) During synaptic release small increases in fluorescence above the relatively high background were observed. After subtracting pre-stimulation from the post-stimulation image, areas of activity became more apparent. For precise localizations of active regions of interests (ROIs), the maximum projection of the first derivative over time of an image stack was obtained after high-pass image filtering (magenta spots in the bottom right panel).

(C) Examples of single-synapse fluorescence traces sampled from raw images in response to electrical stimulation (top) and in the presence of TTX (bottom) to capture spontaneous activities. Scale bars, 10 μm in (A and B).

synapse were similar, with amplitudes in the range of 0.2–0.6 relative change in fluorescence ($\Delta F/F_o$), rise time within a single frame (50 ms), and decay constants on the order of ~100 ms (Figure 2C).

We then compared the spontaneous release amplitude of events occurring within the first minute of the measurement (unbleached unitary quantal amplitude) with the averaged amplitudes of evoked release over a range of probabilities. We see that the ratio of spontaneous to evoked amplitudes starts at one for synapses with low release probability, likely uniquantal evoked release, and decreases with increasing evoked release probability (Figure 2D). This, together with Figure 2B, clearly indicates that even for synapses with moderate evoked release probability, multi-quantal release can occur in dissociated hippocampal culture.

Differences in the distribution of evoked and spontaneous fusion sites

During the measurements of evoked and spontaneous release described above, the maximum intensity projection of the difference image was used to localize active synapses. These often occurred at morphologically distinct regions identifiable as axonal boutons or dendritic spines (Figure 3A). When reviewing images of individual events occurring at an identified synapse, there was strong overlap but often an apparent jitter in the location of release. To characterize whether there are differences in spatial distribution between release modes, we selected synapses with similar numbers of measured evoked cand spontaneous responses and performed subpixel localization of the centroid of release by least-square fitting of a Gaussian distribution to the initial release signal of each event (Figures 3B and 3C) (Ovesny et al., 2014). Evoked release tended to occur within a tight spatial distribution, likely indicating the bounds of the active zone, whereas spontaneous release was more diffuse likely occurring at both the active and periactive zones. Farthest distance between each type of release was computed from 182 synapses. The cumulative distribution of farthest distances shows significantly tighter spatial regulation of evoked release sites when compared with spontaneous release sites (Figure 3D). Although the measurements of spontaneous release do occur over a longer window than those of evoked, there is no dependence of the distance between observed release events and the time between these events (Figure S4). Further analysis of the areas covered by spontaneous and evoked release events (Figure 3E) showed much higher spontaneous release densities outside of evoked release areas (Figure 3F). These data are in complete agreement with a previous study where a significantly smaller evoked fusion area compared with spontaneous fusion sites was observed in pHluorin-based measurements in individual hippocampal boutons (Tang et al., 2016).

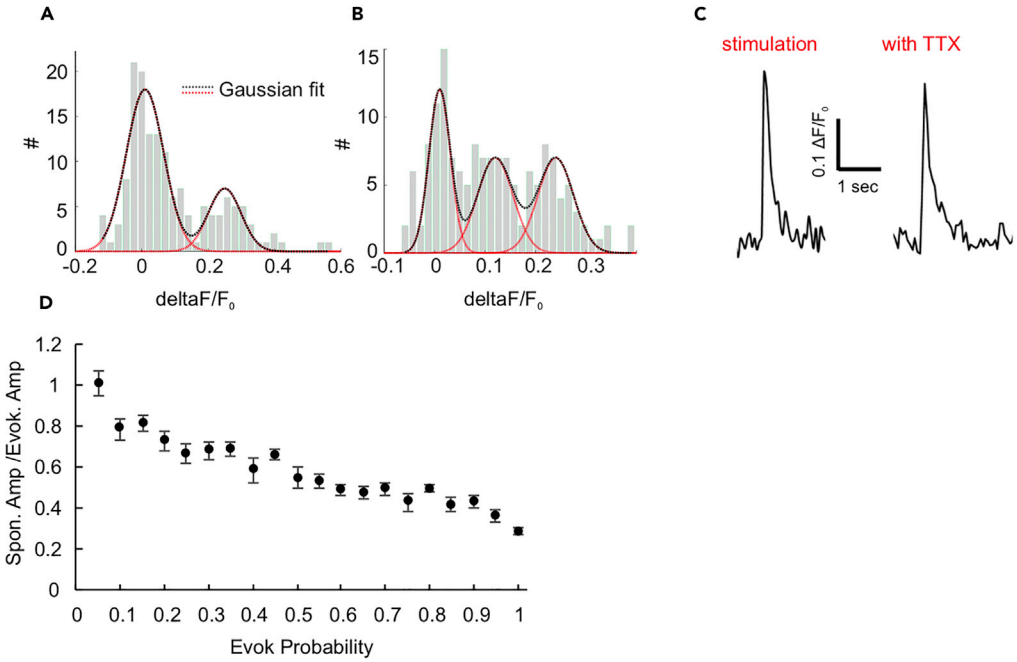

Figure 2. Resolution of unitary release quanta and presence of multivesicular release at individual boutons

(A) The histogram of individual stimulus-evoked fluorescence change amplitudes measured during 0.5-Hz stimulus trains fit well to a sum of Gaussian distributions (black dashed line). The prominent distribution centered at zero represents release failures, and the first non-zero peak represents the unitary quantal amplitude at that synapse.

(B) In approximately 10% boutons, multi-quantal release at individual boutons is indicated by additional distributions centered near integer multiples of the unitary quantal amplitude.

(C) Fluorescence changes during field stimulation-evoked release and AP-independent spontaneous glutamate release show similar rise time, amplitudes, and recovery.

(D) The spontaneous amplitude (acquired during the first minute)/evoking amplitude ratio decreases with increasing evoked release probability, indicating the increased likelihood of multi-quantal release. Error bars represent SEM (n > 1,000 synapses).

Intersynaptic variability in strength of evoked and spontaneous release

From the measurements described above, we could measure the evoked (Figures 4A and 4B) and spontaneous (Figures 4C and 4D) glutamate release events at over 400 individual synapses in a single field of view. By performing these measurements at more than 60 cells, we could characterize the evoked release probability and spontaneous fusion frequency at over 24,000 individual synapses. We obtained an averaged release probability of 0.25 (Figure 4E) and spontaneous frequency of 0.011 Hz (Figure 4F). Excluding synapses that exhibited only spontaneous activity increased the averaged release probability to 0.37, which agrees with the recent Ca^{2+} imaging measurements in hippocampal cultures (Reese and Kavalali 2016). However, as in our measurements evoked probabilities smaller than 0.05 are rounded to zero, it is likely that the true estimate of mean release probability lies in between the two reported values.

Similar to previous observations at the *Drosophila* neuromuscular junction (Melom et al., 2013) and hippocampal synapses (Reese and Kavalali 2016), the distribution of the number of spontaneous events observed within a certain time (5 min) was non-Poisson (Figure S5), implying that the differences measured among synapses is not the result of the same stochastic process. When we plotted the two functional properties of synapses against each other, we observed a remarkable variability. The majority of synapses exhibited both evoked and spontaneous neurotransmission (Figure 4G). No significant correlation (dashed white line in Figure 4G, $R^2 = 0.014$) was observed between the two forms of release, suggesting that discrete mechanisms are employed.

Release properties did seem to be correlated for neighboring hippocampal boutons. We observed large spatial correlation of evoked release probability between synapses with a length constant of 6.7 μm (Figure S6A). For spontaneous frequencies, we observed much smaller correlation between synapses with a shorter

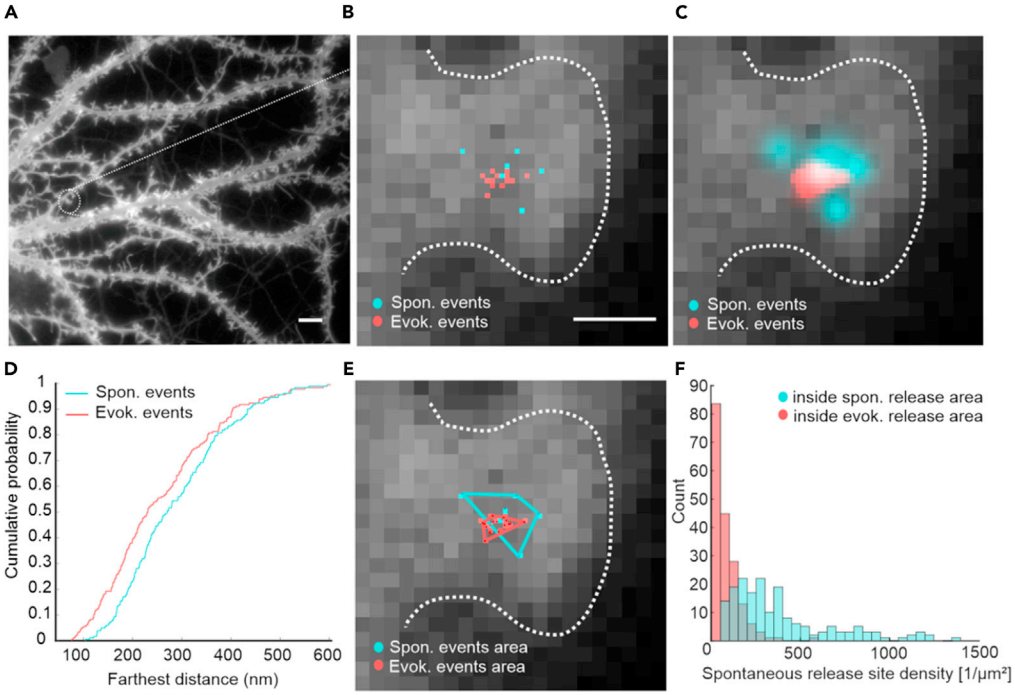

Figure 3. Subpixel localization of evoked and spontaneous release events reveals distinct spatial regulation

(A) To assess the spatial organization of AP-evoked and spontaneous release sites in the same bouton, synapses with at least 10 evoked responses and 5 spontaneous release events were selected.

(B) Sub-pixel coordinates of the release sites for both evoked (red) and spontaneous release events (cyan) were estimated from the centroid of the initial change in fluorescence.

(C) Release site coordinates for evoked (red) and spontaneous (cyan) release site localizations shown as normalized symmetric 2D Gaussian functions with a standard deviation equal to their localization uncertainty. The mean localization uncertainty for fits of evoked and spontaneous release events were 86.9 and 89.5 nm, respectively.

(D) Farthest distances between release sites were computed for evoked and spontaneous release in 182 synapses. The cumulative distribution of farthest distances shows significantly tighter spatial regulation of evoked release sites (Kolmogorov-Smirnov test, p value = 0.008).

(E) The surface areas covered by evoked and spontaneous release events were estimated by the convex hulls around their sub-pixel coordinates.

(F) The density of detected spontaneous release is on average greater inside spontaneous release areas than in evoked release areas. Scale bars: 10 μm in (A) and 1 μm in (B).

length constant of 2.7 μm (Figure S6B). The functional correlation between neighboring synapses has been observed by numerous other studies in both primary cultures (Murthy et al., 1997; Branco et al., 2008; Taschenberger et al., 2016), and tissue slices (Koester and Johnston 2005; Staras et al., 2010). This is likely due to the high probability of adjacent pre-synapses originating from the same axon where inter-synaptic sharing of second messengers, proteins, and SVs have been shown to occur (Darcy et al., 2006; Staras et al., 2010).

Molecular variability among central synapses

To test whether the observed functional variability may be the result of molecular heterogeneity at the synapse, we first characterized the relative expression of a variety of presynaptic proteins including vesicle-associated proteins and Ca^{2+}-sensing and presynaptic soluble proteins at hippocampal synapses. We performed immunolabeling of a given protein of interest and the active zone protein Bassoon (Figures 5A and S7). The punctate Bassoon labeling was used to identify synapses, provide a measure of relative active zone size (Tang et al., 2016), and to identify regions from which the intensity of the other labeled proteins were sampled. The variability of expression relative to Bassoon differed extensively across tested proteins (Figure 5B). To compare the degree to which expression heterogeneity differed among proteins, we computed the Pearson correlation coefficient of the intensity of labeling relative to that of Bassoon. Canonical SV proteins like vesicle-associated membrane protein (VAMP) 2 displayed a relatively tight correlation with Bassoon expression (R^2 = 0.69), whereas some targets, such as VAMP7, were much more

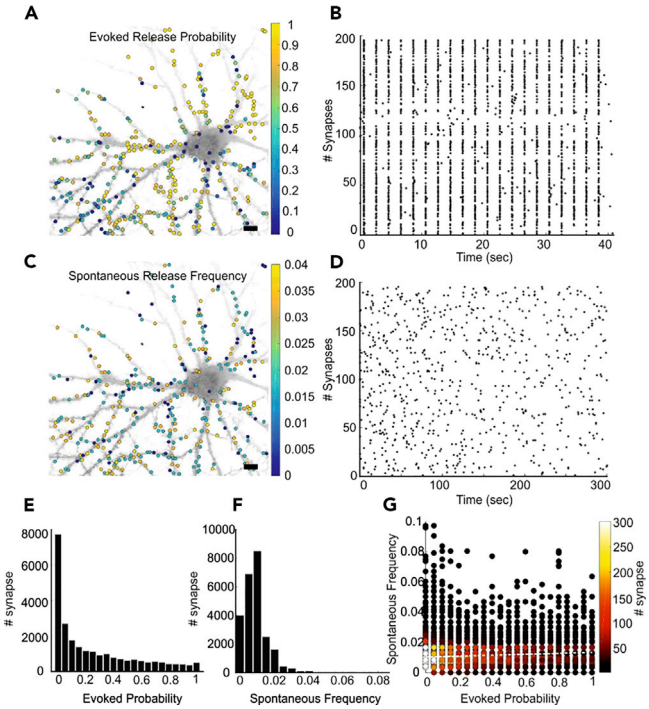

Figure 4. Imaging evoked and spontaneous synaptic release reveals intersynaptic variability of release properties

(A and B) The location of release sites and corresponding evoked release probability, designated by color, of hundreds of active synapses in a single field of view (A) can be computed from release events detected during a train of 20 stimuli applied at 0.5 Hz (B).

(C and D) Spontaneous release frequency is measured in the same sample (C) for 5 min following an initial 5-min incubation in 500 nm TTX (D). Each dot in (B and D) represents one release event.

(E) A histogram of evoked release probability from over ~24,000 individual synapses reveals a mean release probability of 0.25 and a large population (31%) that shows no evoked release.

(F) The histogram of the spontaneous frequency shows a mean of 0.011 Hz.

(G) The evoked release probability and spontaneous release frequency from all measured synapses are plotted in a density-scatter plot. The color represents the number of synapses for which a given pair of values was measured. No correlation was measured between evoked probability and spontaneous frequency (white line, $R^2 = 0.014$). Scale bar: 10 μm in (A and C).

heterogeneously expressed across hippocampal boutons ($R^2 = 0.16$). These measurements revealed varying levels of heterogeneity of individual synaptic proteins (Figures 5C–5E) that when taken together compound into vast heterogeneity in molecular composition at presynaptic boutons.

Relative abundance of synaptic proteins correlates with functional properties

To directly compare the functional properties and molecular composition of synapses, we performed on-stage immuno-labeling following glutamate release imaging. For each measurement, we obtained the evoked probability, the spontaneous release frequency, and the abundance of given protein relative to Bassoon at individual synapses (Figure 6A, compare with Figures 4A and 4C). In line with a previous report (Holderith et al., 2012), we observed a positive correlation between evoked release probability and active-zone size (Bassoon intensity) (Figure 6B). We also show that spontaneous release rate scales with synapse size (Figure 6C). Consistent with the observed intersynaptic spatial correlation of release properties (Figures S6A and S6B), we observed that the amount of Bassoon labeling was also correlated among neighboring synapses with a similar length constant of 5 μm (Figure S6C).

To check for the correlation between release modes and molecular properties of synapses, we divided the synaptic measurements into three equal-sized pools (Figure 6D): (1) a "spontaneous release" pool with no or relatively low evoked release (marked in gray), (2) a "mixed" pool with similar relative of evoked and

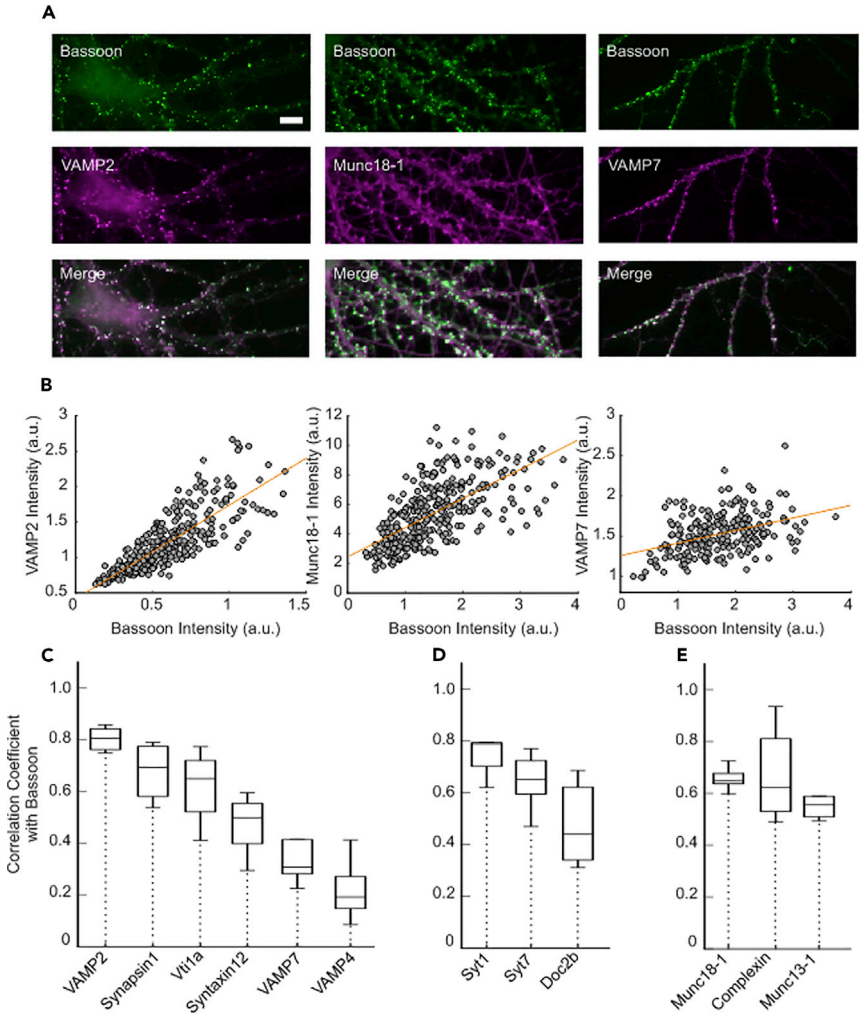

Figure 5. Vast variability in relative molecular expression across central synapses

(A) Representative images of co-labeling for Bassoon and different presynaptic proteins; scale bar, 10 μm.

(B) Flat-field corrected intensities of tested proteins against flat-field corrected Bassoon intensities shows that the expression profile of different presynaptic proteins varies extensively among central synapses (dashed lines represent linear fitting; R^2 for VAMP2, Munc18-1, and VMAP7 are 0.69, 0.42, and 0.16, respectively).

(C–E) Analysis of correlation coefficient between Bassoon and vesicle-associated (C), Ca^{2+}-sensing (D), and presynaptic soluble proteins (E) show the greatest heterogeneity (smallest correlation coefficient) for non-canonical SV proteins (box: first and third quartile, line: median, whiskers: the minimum and maximum values [n = 4–8 cells per protein of interest]).

spontaneous activity and (3) an "evoked release" pool with no or relatively low spontaneous release (marked in blue). To mitigate variation in labeling efficiency between cells, we only compared the relative abundance of each protein within the same experiment (Figures 6E and S8). We were then able to distill these values into the relative enrichment of a protein in spontaneous synapses by dividing their relative abundance in "spontaneous" pool to that of the "evoked release" pool (Figures 6F–6H).

In case of vesicle-associated proteins, we observed more than 1.5-fold enrichment (did not reach statistical significance) of non-canonical N-ethylmaleimide-sensitive factor attachment receptors (SNAREs) proteins, namely, Vti1a and VAMP7, in the "spontaneous" pool synapses, whereas VAMP2, the classical vesicular SNARE, displayed a significant relative enrichment in the "evoking" pool of synapses. Synapsin-1 also showed significant enrichment in the "evoking" synapses (Figure 6F). Among tested Ca^{2+} sensors we observed significant enrichment of Doc2b in the "spontaneous" pool and Synaptotagmin 1 in the "evoked" pool (Figure 6G). Interestingly, all tested presynaptic soluble proteins also showed significantly higher expression in the "spontaneous" pool synapses (Figure 6H).

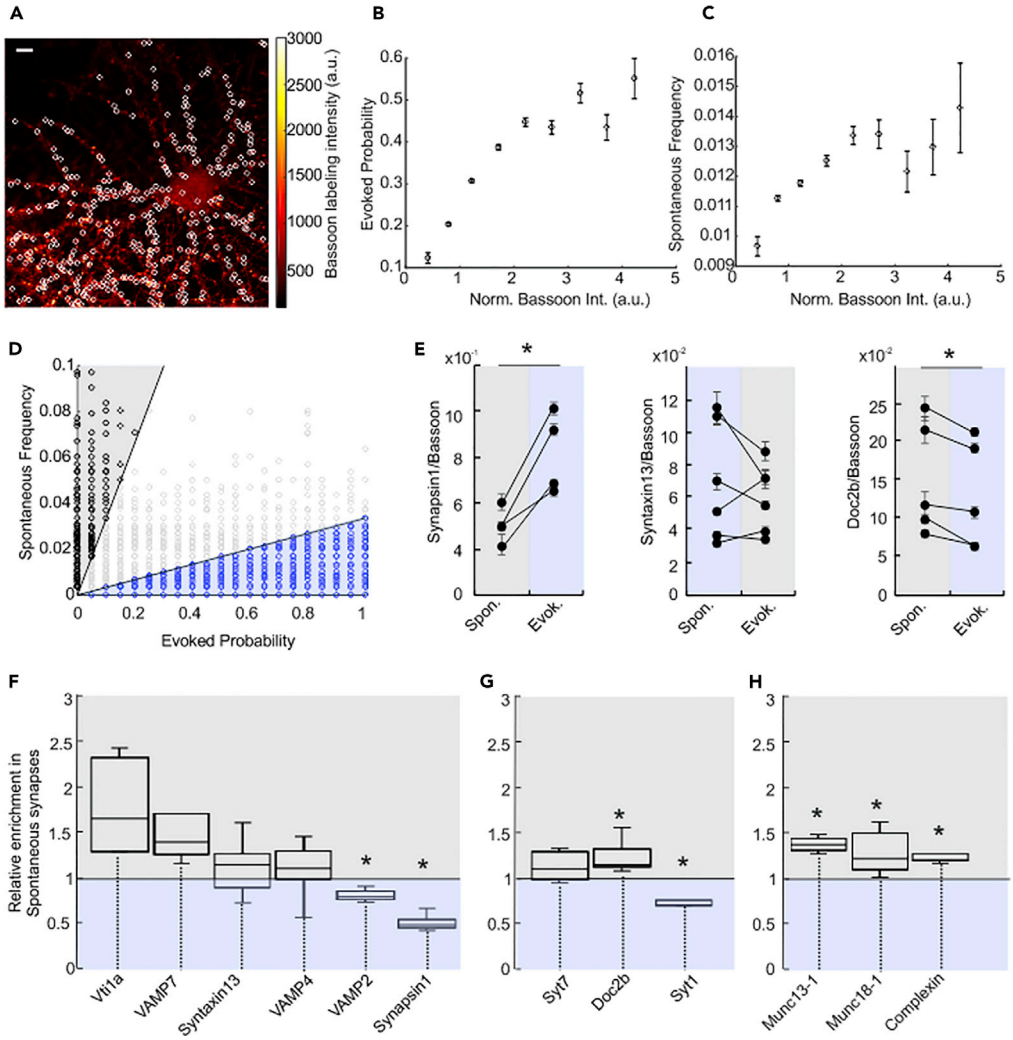

Figure 6. Functional properties of synapse correlate with synapse size and molecular composition

(A) Active synapses (white circles) superimposed on the Bassoon-labeled image (see Figures 4A and 4C, scale bar, 10 μm).

(B) The averaged evoked probabilities of synapses show an increase as the synapse size (estimated by the abundance of Bassoon) increases.

(C) Averaged spontaneous frequencies of hippocampal boutons also scale with their size. Error bars in (B and C) represent SEM (n is on average 1,731 synapses per point).

(D) "Spontaneous" (gray) and "evoked" (blue) pools marked on the scatterplot of the total dataset.

(E) Paired comparison between the relative abundance of each protein in spontaneous synapses and evoked synapses of the same cell (each two black circles connected by a dashed line represent one cell. Error bars represent SEM [n > 100 synapses per black circle]).

(F–H) Relative enrichments of vesicle-associated proteins (F) and Ca^{2+}-sensing (G) and presynaptic soluble proteins (H) in spontaneous synapses (box: first and third quartile, line: median, whiskers: the minimum and maximum values [n = 4–8 cells per protein of interest]).

Discussion

Here we used genetically encoded glutamate sensor to image release at thousands of synapses in neuronal cultures. This enabled us to characterize the variability, interdependency, spatial localization, and molecular regulation of AP-evoked and spontaneous synaptic vesicle exocytosis.

Although still most often used to measure glutamate release during stimulus trains and bursts of activity (Namiki et al., 2007; Marvin et al., 2013) some glutamate imaging work has focused at discrete events at single synapses (Taschenberger et al., 2016). Recently, Sakamoto and colleagues used an enhanced E

(glutamate) optical sensor (EOS) hybrid glutamate sensor to investigate activity at single synapses (Sakamoto et al., 2018). Using fluctuation analysis, they were able to fit a binomial model of glutamate release at the synapse to determine quantal parameters. With iGluSnFR, we show that the signal amplitude from evoked release synapses with low evoked probability is equivalent to that released during spontaneous fusion. We obtained the same results with a new variant of iGluSnFR (Figure S9), which became available during the time course of our study (Marvin et al., 2018; Jensen et al., 2019). With both sensors, we also clearly show that increasing the evoked release probability results in an increase in amplitude compared with spontaneous "mini" amplitude indicating that multi-quantal release occurs in small synapses, even at relatively low evoked probabilities (Figures 2D and S9B).

It should be noted that our interpretation of these data is based on the assumption that release events are happening at individual synapses. It has been shown that multi-synapse aggregates do exist in culture (Kavalali et al., 1999; Welzel et al., 2010). However, the coefficient of variation (CV) for our estimates of active zone size, based on Bassoon labeling (Figure S10, CV = 0.5), are in close agreement with the single active zone area distribution measured by electron microscopy (EM) (CV = 0.56 and 0.7 in brain slices and culture, respectively, Schikorski and Stevens 1997), indicating that the vast majority of sites from which we measure activity are single synapses.

Typically, our measurements provide coverage of most of the dendritic arbor of a cultured neuron (219 μm × 219 μm field of view), capturing activity of hundreds of synapses in a single experiment. This enhanced throughput allowed us to characterize the evoked release probability and spontaneous fusion frequency in more than 24,000 synapses. Early work using styryl dyes reported tight correlation of evoked and spontaneous activity at individual synapses (Prange and Murphy 1999, $r = 0.59$; $p < 0.0001$). This work concluded that both forms of release were regulated in parallel, originating from the same pool of readily releasable vesicles and utilizing the common release machinery. However, more recent studies at the *Drosophila* neuromuscular junction offered conflicting reports. One group reported on a negative correlation between these properties (Peled et al., 2014) suggesting that highly active synapses preferred one mode of transmission, whereas the others concluded that these properties were poorly correlated (Melom et al., 2013). Work that utilized postsynaptic calcium measurements in hippocampal cultures also indicated that these properties are poorly correlated (Reese and Kavalali 2016, $R^2 = 0.012$). Our results, confirm that there is no positive or negative correlation ($R^2 = 0.014$) between evoked and spontaneous release probability in hippocampal boutons. This would indicate that, for the most part, these forms of release are independently regulated.

That is not to say that evoked and spontaneous release are completely free from co-regulation. It is well established that synaptic structure is a major factor regulating synaptic release. Evoked and spontaneous release efficiency is known to scale with vesicle pool size (Murthy et al., 1997). Evoked release has also been shown to scale with active zone area (Holderith et al., 2012). Indeed, our results indicate that both evoked (Figure 6B) and spontaneous release (Figure 6C) scale with active zone size in hippocampal boutons. The existence of scaling with active zone size for both forms of release, yet lack of correlation between the properties, provides additional support of the presence of other stronger mechanisms of differential regulation.

The ultrastructural organization within a synapse also regulates exocytosis. Tight spatial coupling of primed vesicles to voltage-gated calcium channels is essential for synchronous evoked release (Eggermann et al., 2011). Many synapses employ specialized structures such as ribbons or T-bars to facilitate vesicle clustering and coupling to calcium channels to further increase evoked release fidelity (Ackermann et al., 2015). The spatial regulation of spontaneous release, however, remains poorly understood. Work in the large ribbon synapses of retinal bipolar (Zenisek 2008) and photoreceptors cells (Cork et al., 2016) has shown differences in spontaneous fusion rates across the synapse. The ribbon is the predominant site of evoked release, whereas higher rates of spontaneous release occurred at non-ribbon sites. Based on the subpixel localization of evoked and spontaneous glutamate release, we also observed significant differences in spatial distribution of evoked and spontaneous release sites. We show that spontaneous release occurs over a larger area of hippocampal boutons than evoked release (Figures 3B–3F) and with higher frequency outside the bounds of evoked release. Super-resolution imaging has shown tight clustering of active zone proteins at discrete release sites of hippocampal boutons (Sakamoto et al., 2018). Similarly, tight sequestration and peripheral depletion of factors responsible for spontaneous release clamping (Schupp et al., 2016), could leave peripheral vesicles more susceptible to spontaneous exocytosis. Together with the previously shown transsynaptic alignment of postsynaptic receptors at the fusion sites (Tang et al., 2016), this spatial

regulation of spontaneous and evoked release sites could explain how these release modes preferentially activate non-overlapping populations of postsynaptic receptors (Atasoy et al., 2008; Sara et al., 2011).

It should be noted, that the subset of synapses selected for subpixel localization possessed above average release properties to provide sufficient event localizations for comparison of evoked and release distribution. It is likely that release properties and release localization distribution are interdependent and there may be combinations of evoked and spontaneous release properties where the observations presented in Figure 3 do not hold. Future investigation using this same experimental framework may provide insight into these dependencies as well as the dynamics of release site localization during synaptic maturation or plasticity.

Several decades of work, mostly reliant on genetic manipulation, has provided a solid foundation for the molecular regulation of synaptic release. This past work has identified a number of factors that are essential for SV exocytosis and others that serve more modulatory roles. We show that a number of vesicle-associated, calcium-sensing, and soluble presynaptic proteins are present at dramatically different levels across synapses. For some of the tested proteins, we noticed that in addition to the established presynaptic localization, apparent dendritic staining was observed (Figures 5 and S7). Nevertheless, by performing post hoc immunolabeling of synapses that show more relative spontaneous activity, more relative evoked release, or equal contributions to both forms of release, we were able to show that for a number of these proteins their abundance relative to Bassoon does correlate with presynaptic function. Although we show that iGluSnFR is able to reliably report on the spontaneous release events, the window over which sufficient signal to noise ratio (SNR) is achieved is limited. This, in turn, limits the resolution with which release frequency can be measured. With a median number of observed spontaneous events of approximately 3 per 5-min window the confidence of spontaneous release frequency and thus molecular and spatial correlates for a single synapse may be low. However, we show that by pooling thousands of synapses by their evoked and spontaneous release properties significant molecular correlations become apparent.

VAMP2 and synaptotagmin 1, whose absence results in severe decrease in AP-evoked SV fusion (Geppert et al., 1994; Schoch et al., 2001; Chapman 2008) displayed significantly greater relative abundance in synapses that tend to have relatively stronger evoked release. Similarly, Synapsin 1 was found to be expressed to a greater extent at synapses with relative higher evoked probabilities. Synapsin 1 plays an important role in evoked neurotransmission by tightening the vesicular release to physiological stimuli (Chi et al., 2003); however, spontaneous release has been reported to stay unchanged after its loss (Chiappalone et al., 2009).

Doc2b, on the other hand, was found to be enriched in synapses with higher relative spontaneous fusion. Doc2b has been proposed to be a calcium sensor for spontaneous release (Groffen et al., 2010) and a calcium-independent enhancer of spontaneous release (Pang et al., 2011). In addition, two vesicle-associated membrane proteins, Vti1a and VAMP7, showed higher expression in synapses with higher relative spontaneous release but did not show significant enrichment. In addition to their roles in fusion of intracellular organelles such as late endosomes (Medigeshi and Schu 2003; Ganley et al., 2008) and lysosomes (Pryor et al., 2004), these proteins are proposed to define a "spontaneous pool" of SVs (Hua et al., 2011; Ramirez et al., 2012; Bal et al., 2013). The abundance of Vti1a was shown to correlate with spontaneous release activity, and its loss selectively reduced spontaneous neurotransmission (Ramirez et al., 2012). Vamp7, however, is proposed to regulate asynchronous release as well (Scheuber et al., 2006), which might explain its lower enrichment when compared with Vti1a at synapses with higher relative spontaneous activity.

Surprisingly the three soluble synaptic proteins we tested, Munc13, Munc18, and Complexin, were found to be significantly enriched in synapses with stronger relative spontaneous release. Munc18 and Munc13 cooperate to prime the ternary SNARE complex (Lai et al., 2017). In Munc18-1-deficient mice and Munc13-1/2 double knockout mice both evoked and spontaneous synaptic neurotransmitter release are completely abolished (Verhage et al., 2000; Varoqueaux et al., 2002). Our results indicate that excess abundance of these factors, relative to Bassoon, leads to enhanced spontaneous release. Munc13 has been shown to tightly cluster around sites of evoked release (Sakamoto et al., 2018). It may be the case that when local abundance of a protein exceeds that of other active zone proteins (i.e., Bassoon), the capacity to effectively sequester it within evoked release sites is diminished. Then excess Munc13 and Munc18 are free to dock and prime vesicles outside of the organized active zone, where we show more spontaneous release occur. This provides insight into why phorbol esters, that potentiate all release through Munc13 (Rhee et al., 2002), have been shown to specifically enhance spontaneous release outside of organized release sites (Zenisek 2008).

Despite a history of conflicting reports, Complexin is now believed to interact with the trans-SNARE complex to regulate the energetic requirements for SV fusion. Whether this interaction clamps or triggers SV fusion seems to depends on the isoform of protein, the synapse type, as well as the model system used in the study (Neher 2010; Trimbuch and Rosenmund 2016). Our results showing an enrichment of Complexin in synapses with higher relative spontaneous activity suggests a facilitatory role for Complexin, in line with numerous other works (Xue et al., 2008; Strenzke et al., 2009; Xue et al., 2010; Chang et al., 2015). Most recently, fluorescence resonance energy transfer assay using mammalian proteins has shown that although it is not essential to form the primed state of the trans-SNARE complex, Complexin, together with Munc13 and Munc18, protects it from disassembly (Prinslow et al., 2019). It would follow that synapses with greater abundance of these factors would have a greater number of primed vesicles available for release.

Taken together, our results show that the regulation of evoked and spontaneous release occurs at many different levels that, when combined, result in vast functional variability across synapses. It is evident that further resolution of the coordinated and divergent mechanisms will require greater resolution of key molecules within the ultrastructure of the synapse. The combination of functional optical assays, such as the glutamate release imaging used in this work, together with multicolor super-resolution techniques, will allow us to better understand how molecular ultrastructure governs the strength of different release modes at the synapse.

Limitations of the study

As with most works that utilize fluorescent indicators, particularly genetically encoded indicators, the characterization of synaptic release in this work is limited by the finite photon budget of iGluSnFR. Care was taken to find an optimal balance between spatial, temporal, and signal resolution in the detection of synaptic release. Indeed, sufficient SNR was achieved to resolve unitary release events. Measurements of evoked release allowed us to assign synaptic release probabilities in 5% intervals. However, the window over which sufficient SNR was maintained while measuring spontaneous release was limited to 5 min. During this time the vast majority of the synapses exhibiting fewer than five spontaneous release events, resulting in courser discretization of spontaneous release frequency. Several groups are working to further optimize glutamate sensors to increase their brightness and modulate their affinity. These advancements together with advanced imaging methods, such as targeted illumination, may increase our photon budget and thus the amount of information about glutamate release one is able to gather from a single synapse.

Resource availability

Lead contact

Further information and requests for resources and reagent should be directed to the Lead Contact Andrew Woehler (andrew.woehler@mdc-berlin.de).

Material availability

This study did not generate any new or unique reagents.

Data and code availability

The datasets and code supporting the current study have not been deposited in a public repository due to their size but are available from the corresponding author upon request.

Methods

All methods can be found in the accompanying Transparent methods supplemental file.

Supplemental information

Supplemental information can be found online at https://doi.org/10.1016/j.isci.2020.101909.

Acknowledgments

We would like to thank Erwin Neher and Reinhard Jahn for their comments on the manuscript. Also, we thank Dr. Tolga Soykan for his technical assistance. This work was supported by the Peter und Traudl Engelhorn Stiftung through a post-doc stipend to Z.F.

Author contributions

A.W. conceived the project. A.W. and F.P. performed preliminary experiments. Z.F. performed the experiments and data analysis. A.E.K. prepared neuronal cultures and assisted with immune-labeling experiments. M.W. performed sub-pixel localization analysis. A.W., Z.F., and M.W. evaluated the results. A.W. and Z.F wrote the manuscript.

Declaration of interests

The authors declare that they have no competing interests.

Received: June 29, 2020
Revised: September 24, 2020
Accepted: December 3, 2020
Published: January 22, 2021

References

Ackermann, F., Waites, C.L., and Garner, C.C. (2015). Presynaptic active zones in invertebrates and vertebrates. EMBO Rep. *16*, 923–938.

Akaike, H. (1973). Information Theory and an Extension of the Maximum Likelihood Principle. In 2nd International Symposium on Information Theory (Akadémiai Kiadó), pp. 199–213.

Atasoy, D., Ertunc, M., Moulder, K.L., Blackwell, J., Chung, C., Su, J., and Kavalali, E.T. (2008). Spontaneous and evoked glutamate release activates two populations of NMDA receptors with limited overlap. J. Neurosci. *28*, 10151–10166.

Bal, M., Leitz, J., Reese, A.L., Ramirez, D.M., Durakoglugil, M., Herz, J., Monteggia, L.M., and Kavalali, E.T. (2013). Reelin mobilizes a VAMP7-dependent synaptic vesicle pool and selectively augments spontaneous neurotransmission. Neuron *80*, 934–946.

Branco, T., Staras, K., Darcy, K.J., and Goda, Y. (2008). Local dendritic activity sets release probability at hippocampal synapses. Neuron *59*, 475–485.

Chang, S., Reim, K., Pedersen, M., Neher, E., Brose, N., and Taschenberger, H. (2015). Complexin stabilizes newly primed synaptic vesicles and prevents their premature fusion at the mouse calyx of held synapse. J. Neurosci. *35*, 8272–8290.

Chapman, E.R. (2008). How does synaptotagmin trigger neurotransmitter release? Annu. Rev. Biochem. *77*, 615–641.

Chi, P., Greengard, P., and Ryan, T.A. (2003). Synaptic vesicle mobilization is regulated by distinct synapsin I phosphorylation pathways at different frequencies. Neuron *38*, 69–78.

Chiappalone, M., Casagrande, S., Tedesco, M., Valtorta, F., Baldelli, P., Martinoia, S., and Benfenati, F. (2009). Opposite changes in glutamatergic and GABAergic transmission underlie the diffuse hyperexcitability of synapsin I-deficient cortical networks. Cereb. Cortex *19*, 1422–1439.

Cork, K.M., Van Hook, M.J., and Thoreson, W.B. (2016). Mechanisms, pools, and sites of spontaneous vesicle release at synapses of rod and cone photoreceptors. Eur. J. Neurosci. *44*, 2015–2027.

Darcy, K.J., Staras, K., Collinson, L.M., and Goda, Y. (2006). Constitutive sharing of recycling synaptic vesicles between presynaptic boutons. Nat. Neurosci. *9*, 315–321.

Dobrunz, L.E., and Stevens, C.F. (1997). Heterogeneity of release probability, facilitation, and depletion at central synapses. Neuron *18*, 995–1008.

Eggermann, E., Bucurenciu, I., Goswami, S.P., and Jonas, P. (2011). Nanodomain coupling between Ca(2)(+) channels and sensors of exocytosis at fast mammalian synapses. Nat. Rev. Neurosci. *13*, 7–21.

Fatt, P., and Katz, B. (1952). Spontaneous subthreshold activity at motor nerve endings. J. Physiol. *117*, 109–128.

Fredj, N.B., and Burrone, J. (2009). A resting pool of vesicles is responsible for spontaneous vesicle fusion at the synapse. Nat. Neurosci. *12*, 751–758.

Ganley, I.G., Espinosa, E., and Pfeffer, S.R. (2008). A syntaxin 10-SNARE complex distinguishes two distinct transport routes from endosomes to the trans-Golgi in human cells. J. Cell Biol. *180*, 159–172.

Geiger, J.R., and Jonas, P. (2000). Dynamic control of presynaptic Ca(2+) inflow by fast-inactivating K(+) channels in hippocampal mossy fiber boutons. Neuron *28*, 927–939.

Geppert, M., Goda, Y., Hammer, R.E., Li, C., Rosahl, T.W., Stevens, C.F., and Sudhof, T.C. (1994). Synaptotagmin I: a major Ca2+ sensor for transmitter release at a central synapse. Cell *79*, 717–727.

Groemer, T.W., and Klingauf, J. (2007). Synaptic vesicles recycling spontaneously and during activity belong to the same vesicle pool. Nat. Neurosci. *10*, 145–147.

Groffen, A.J., Martens, S., Diez Arazola, R., Cornelisse, L.N., Lozovaya, N., de Jong, A.P., Goriounova, N.A., Habets, R.L., Takai, Y., Borst, J.G., et al. (2010). Doc2b is a high-affinity Ca2+ sensor for spontaneous neurotransmitter release. Science *327*, 1614–1618.

Harata, N., Ryan, T.A., Smith, S.J., Buchanan, J., and Tsien, R.W. (2001). Visualizing recycling synaptic vesicles in hippocampal neurons by FM 1-43 photoconversion. Proc. Natl. Acad. Sci. U S A *98*, 12748–12753.

Holderith, N., Lorincz, A., Katona, G., Rozsa, B., Kulik, A., Watanabe, M., and Nusser, Z. (2012). Release probability of hippocampal glutamatergic terminals scales with the size of the active zone. Nat. Neurosci. *15*, 988–997.

Hua, Y., Sinha, R., Martineau, M., Kahms, M., and Klingauf, J. (2010). A common origin of synaptic vesicles undergoing evoked and spontaneous fusion. Nat. Neurosci. *13*, 1451–1453.

Hua, Z., Leal-Ortiz, S., Foss, S.M., Waites, C.L., Garner, C.C., Voglmaier, S.M., and Edwards, R.H. (2011). v-SNARE composition distinguishes synaptic vesicle pools. Neuron *71*, 474–487.

Jensen, T.P., Zheng, K., Cole, N., Marvin, J.S., Looger, L.L., and Rusakov, D.A. (2019). Multiplex imaging relates quantal glutamate release to presynaptic Ca(2+) homeostasis at multiple synapses in situ. Nat. Commun. *10*, 1414.

Kavalali, E.T., Klingauf, J., and Tsien, R.W. (1999). Activity-dependent regulation of synaptic clustering in a hippocampal culture system. Proc. Natl. Acad. Sci. U S A *96*, 12893–12900.

Koester, H.J., and Johnston, D. (2005). Target cell-dependent normalization of transmitter release at neocortical synapses. Science *308*, 863–866.

Lai, Y., Choi, U.B., Leitz, J., Rhee, H.J., Lee, C., Altas, B., Zhao, M., Pfuetzner, R.A., Wang, A.L., Brose, N., et al. (2017). Molecular mechanisms of synaptic vesicle priming by Munc13 and Munc18. Neuron *95*, 591–607.e510.

Leitz, J., and Kavalali, E.T. (2014). Fast retrieval and autonomous regulation of single spontaneously recycling synaptic vesicles. Elife *3*, e03658.

Llinas, R., Sugimori, M., Chu, D., Morita, M., Blasi, J., Herreros, J., Jahn, R., and Marsal, J. (1994). Transmission at the squid giant synapse was blocked by tetanus toxin by affecting synaptobrevin, a vesicle-bound protein. J. Physiol. *477*, 129–133.

Malagon, G., Miki, T., Llano, I., Neher, E., and Marty, A. (2016). Counting vesicular release events reveals binomial release statistics at single glutamatergic synapses. J. Neurosci. *36*, 4010–4025.

Marvin, J.S., Borghuis, B.G., Tian, L., Cichon, J., Harnett, M.T., Akerboom, J., Gordus, A., Renninger, S.L., Chen, T.W., Bargmann, C.I., et al. (2013). An optimized fluorescent probe for visualizing glutamate neurotransmission. Nat. Methods *10*, 162–170.

Marvin, J.S., Scholl, B., Wilson, D.E., Podgorski, K., Kazemipour, A., Muller, J.A., Schoch, S., Quiroz, F.J.U., Rebola, N., Bao, H., et al. (2018). Stability, affinity, and chromatic variants of the glutamate sensor iGluSnFR. Nat. Methods *15*, 936–939.

McLachlan, G., and Peel, D. (2000). Fitting Mixture Models to Binned Data (John Wiley & Sons, Inc).

Medigeshi, G.R., and Schu, P. (2003). Characterization of the in vitro retrograde transport of MPR46. Traffic *4*, 802–811.

Melom, J.E., Akbergenova, Y., Gavornik, J.P., and Littleton, J.T. (2013). Spontaneous and evoked release are independently regulated at individual active zones. J. Neurosci. *33*, 17253–17263.

Murthy, V.N., Sejnowski, T.J., and Stevens, C.F. (1997). Heterogeneous release properties of visualized individual hippocampal synapses. Neuron *18*, 599–612.

Namiki, S., Sakamoto, H., Iinuma, S., Iino, M., and Hirose, K. (2007). Optical glutamate sensor for spatiotemporal analysis of synaptic transmission. Eur. J. Neurosci. *25*, 2249–2259.

Neher, E. (2010). Complexin: does it deserve its name? Neuron *68*, 803–806.

Okubo, Y., Sekiya, H., Namiki, S., Sakamoto, H., Iinuma, S., Yamasaki, M., Watanabe, M., Hirose, K., and Iino, M. (2010). Imaging extrasynaptic glutamate dynamics in the brain. Proc. Natl. Acad. Sci. U S A *107*, 6526–6531.

Ovesny, M., Krizek, P., Borkovec, J., Svindrych, Z., and Hagen, G.M. (2014). ThunderSTORM: a comprehensive ImageJ plug-in for PALM and STORM data analysis and super-resolution imaging. Bioinformatics *30*, 2389–2390.

Pang, Z.P., Bacaj, T., Yang, X., Zhou, P., Xu, W., and Sudhof, T.C. (2011). Doc2 supports spontaneous synaptic transmission by a Ca(2+)-independent mechanism. Neuron *70*, 244–251.

Peled, E.S., Newman, Z.L., and Isacoff, E.Y. (2014). Evoked and spontaneous transmission favored by distinct sets of synapses. Curr. Biol. *24*, 484–493.

Prange, O., and Murphy, T.H. (1999). Correlation of miniature synaptic activity and evoked release probability in cultures of cortical neurons. J. Neurosci. *19*, 6427–6438.

Prinslow, E.A., Stepien, K.P., Pan, Y.Z., Xu, J., and Rizo, J. (2019). Multiple factors maintain assembled trans-SNARE complexes in the presence of NSF and alphaSNAP. Elife *8*, e38880.

Pryor, P.R., Mullock, B.M., Bright, N.A., Lindsay, M.R., Gray, S.R., Richardson, S.C., Stewart, A., James, D.E., Piper, R.C., and Luzio, J.P. (2004). Combinatorial SNARE complexes with VAMP7 or VAMP8 define different late endocytic fusion events. EMBO Rep. *5*, 590–595.

Ramirez, D.M., Khvotchev, M., Trauterman, B., and Kavalali, E.T. (2012). Vti1a identifies a vesicle pool that preferentially recycles at rest and maintains spontaneous neurotransmission. Neuron *73*, 121–134.

Reese, A.L., and Kavalali, E.T. (2016). Single synapse evaluation of the postsynaptic NMDA receptors targeted by evoked and spontaneous neurotransmission. Elife *5*, e21170.

Rhee, J.S., Betz, A., Pyott, S., Reim, K., Varoqueaux, F., Augustin, I., Hesse, D., Sudhof, T.C., Takahashi, M., Rosenmund, C., and Brose, N. (2002). Beta phorbol ester- and diacylglycerol-induced augmentation of transmitter release is mediated by Munc13s and not by PKCs. Cell *108*, 121–133.

Sakamoto, H., Ariyoshi, T., Kimpara, N., Sugao, K., Taiko, I., Takikawa, K., Asanuma, D., Namiki, S., and Hirose, K. (2018). Synaptic weight set by Munc13-1 supramolecular assemblies. Nat. Neurosci. *21*, 41–49.

Sara, Y., Bal, M., Adachi, M., Monteggia, L.M., and Kavalali, E.T. (2011). Use-dependent AMPA receptor block reveals segregation of spontaneous and evoked glutamatergic neurotransmission. J. Neurosci. *31*, 5378–5382.

Sara, Y., Virmani, T., Deak, F., Liu, X., and Kavalali, E.T. (2005). An isolated pool of vesicles recycles at rest and drives spontaneous neurotransmission. Neuron *45*, 563–573.

Scheuber, A., Rudge, R., Danglot, L., Raposo, G., Binz, T., Poncer, J.C., and Galli, T. (2006). Loss of AP-3 function affects spontaneous and evoked release at hippocampal mossy fiber synapses. Proc. Natl. Acad. Sci. U S A *103*, 16562–16567.

Schikorski, T., and Stevens, C.F. (1997). Quantitative ultrastructural analysis of hippocampal excitatory synapses. J. Neurosci. *17*, 5858–5867.

Schoch, S., Deak, F., Konigstorfer, A., Mozhayeva, M., Sara, Y., Sudhof, T.C., and Kavalali, E.T. (2001). SNARE function analyzed in synaptobrevin/VAMP knockout mice. Science *294*, 1117–1122.

Schupp, M., Malsam, J., Ruiter, M., Scheutzow, A., Wierda, K.D., Sollner, T.H., and Sorensen, J.B. (2016). Interactions between SNAP-25 and synaptotagmin-1 are involved in vesicle priming, clamping spontaneous and stimulating evoked neurotransmission. J. Neurosci. *36*, 11865–11880.

Staras, K., Branco, T., Burden, J.J., Pozo, K., Darcy, K., Marra, V., Ratnayaka, A., and Goda, Y. (2010). A vesicle superpool spans multiple presynaptic terminals in hippocampal neurons. Neuron *66*, 37–44.

Strenzke, N., Chanda, S., Kopp-Scheinpflug, C., Khimich, D., Reim, K., Bulankina, A.V., Neef, A., Wolf, F., Brose, N., Xu-Friedman, M.A., and Moser, T. (2009). Complexin-I is required for high-fidelity transmission at the endbulb of Held auditory synapse. J. Neurosci. *29*, 7991–8004.

Sutton, M.A., and Schuman, E.M. (2005). Local translational control in dendrites and its role in long-term synaptic plasticity. J. Neurobiol. *64*, 116–131.

Tang, A.H., Chen, H., Li, T.P., Metzbower, S.R., MacGillavry, H.D., and Blanpied, T.A. (2016). A trans-synaptic nanocolumn aligns neurotransmitter release to receptors. Nature *536*, 210–214.

Taschenberger, H., Woehler, A., and Neher, E. (2016). Superpriming of synaptic vesicles as a common basis for intersynapse variability and modulation of synaptic strength. Proc. Natl. Acad. Sci. U S A *113*, E4548–E4557.

Trimbuch, T., and Rosenmund, C. (2016). Should I stop or should I go? The role of complexin in neurotransmitter release. Nat. Rev. Neurosci. *17*, 118–125.

Varoqueaux, F., Sigler, A., Rhee, J.S., Brose, N., Enk, C., Reim, K., and Rosenmund, C. (2002). Total arrest of spontaneous and evoked synaptic transmission but normal synaptogenesis in the absence of Munc13-mediated vesicle priming. Proc. Natl. Acad. Sci. U S A *99*, 9037–9042.

Verhage, M., Maia, A.S., Plomp, J.J., Brussaard, A.B., Heeroma, J.H., Vermeer, H., Toonen, R.F., Hammer, R.E., van den Berg, T.K., Missler, M., et al. (2000). Synaptic assembly of the brain in the absence of neurotransmitter secretion. Science *287*, 864–869.

von Gersdorff, H., and Borst, J.G. (2002). Short-term plasticity at the calyx of Held. Nat. Rev. Neurosci. *3*, 53–64.

Waters, J., and Smith, S.J. (2002). Vesicle pool partitioning influences presynaptic diversity and weighting in rat hippocampal synapses. J. Physiol. *541*, 811–823.

Welzel, O., Tischbirek, C.H., Jung, J., Kohler, E.M., Svetlitchny, A., Henkel, A.W., Kornhuber, J., and Groemer, T.W. (2010). Synapse clusters are preferentially formed by synapses with large recycling pool sizes. PLoS One *5*, e13514.

Wilhelm, B.G., Groemer, T.W., and Rizzoli, S.O. (2010). The same synaptic vesicles drive active and spontaneous release. Nat. Neurosci. *13*, 1454–1456.

Xue, M., Craig, T.K., Xu, J., Chao, H.T., Rizo, J., and Rosenmund, C. (2010). Binding of the complexin N terminus to the SNARE complex potentiates synaptic-vesicle fusogenicity. Nat. Struct. Mol. Biol. *17*, 568–575.

Xue, M., Stradomska, A., Chen, H., Brose, N., Zhang, W., Rosenmund, C., and Reim, K. (2008). Complexins facilitate neurotransmitter release at excitatory and inhibitory synapses in mammalian central nervous system. Proc. Natl. Acad. Sci. U S A *105*, 7875–7880.

Zenisek, D. (2008). Vesicle association and exocytosis at ribbon and extraribbon sites in retinal bipolar cell presynaptic terminals. Proc. Natl. Acad. Sci. U S A *105*, 4922–4927.

iScience, Volume *24*

Supplemental Information

Single synapse glutamate imaging reveals multiple levels of release mode regulation in mammalian synapses

Zohreh Farsi, Marie Walde, Agnieszka E. Klementowicz, Foteini Paraskevopoulou, and Andrew Woehler

Supplementary Information

Transparent Methods

Constructs

pAAV.hSyn.iGluSnFr.WPRE.SV40 and pCMV(MinDis).iGluSnFR were a gift from Loren Looger (Addgene plasmid # 41732 ; http://n2t.net/addgene:41732 ; RRID:Addgene_41732, and Addgene viral prep # 98929-AAV1; http://n2t.net/addgene:98929 ; RRID:Addgene_98929, respectively) (Marvin, Borghuis et al. 2013). pAAV.hSynapsin.SF-iGluSnFR.A184S was a gift from Loren Looger (Addgene viral prep # 106174-AAV1 ; http://n2t.net/addgene:106174 ; RRID:Addgene_106174).

Neuronal cultures

Primary hippocampal cultures were prepared from postnatal day 0 (P0) rat brains as described previously (Kruger, Favaro et al. 2013), and immobilized on poly-D-Lysine (PDL)-coated glass coverslips. For dendritic measurements, neurons were infected at 2-4 day *in vitro* (DIV) with an adeno-virus associated construct (pAAV.hSyn.iGluSnFr.WPRE.SV40 (Marvin, Borghuis et al. 2013) to express the sensor at the surface of the neurons under human synapsin-1 promoter. The infected cells were then recorded at 17-21 DIV.

For axonal measurements, sparse expression of iGluSnFR in cultured neurons was achieved by transfection of pCMV(MinDis). iGluSnFR construct (Marvin, Borghuis et al. 2013) at 4-7 DIV using Lipofectamine, 2000 (Invitrogen) following the manufacturer's instructions. Imaging was performed on a labeled cell whose neighboring cells were not fluorescent.

For SF-iGluSnFR measurements, neurons were infected at 2-4 DIV with pAAV.hSynapsin.SF-iGluSnFR.A184S, and imaged at 17-21 DIV.

Image acquisition

All the experiments were performed at room temperature in Tyrode's buffer (120 mM NaCl, 2.5mM KCl, 10 mM glucose, 10 mM HEPES, pH 7.4, osmolality was adjusted to that of the culture medium with sucrose). To perform action potential-evoked glutamate release, we used a custom-made imaging chamber with two electrodes for electrical stimulation. The imaging chamber was mounted on the stage of a Nikon Eclipse Ti inverted microscope equipped with a PFS focus controller, a prime 95B scientific CMOS (Photometrics) camera and a pulse generator (HSE-HA, Harvard Apparatus). Illumination was provided in epifluorescence mode by a Lumen 200 Fluorescence Illumination System (Prior Scientific) using a 485/20-nm bandpass filter and emission was collected through a

60x, 1.49 NA Nikon Apochromat objective using a quadband (405/488/561/647nm, Chroma 89902) emission filter. Optical recording of evoked glutamate release was performed by continuous imaging at 20 Hz after application of 20 field stimuli at 0.5 Hz in the presence of 50 µM AP5 (l-2-amino-5-phosphonovaleric acid) and 10 µM CNQX (6-cyano-7-nitroquinoxaline-2,3-dione), to block recurrent network activity. The stimuli were triggered by computer-controlled TTL output and their timing was programmed in VisiView software (Visitron Systems). To be able to sample synapses with different evoked release probabilities, imaging solution was supplemented with 2 mM $CaCl_2$ and 2 mM $MgCl_2$. Spontaneous events were then captured by 5-min continuous imaging at 20 Hz at 4mM $CaCl_2$, in the presence of 0.5 µM tetrodotoxin (TTX) to block action potential firing.

Immuno-labeling

To perform on-stage immune-labeling, we fixed cultured neurons for 10 min with 4% paraformaldehyde immediately after functional imaging. Blocking and permeabilization was performed by 30-min incubation in 2.5% (w/v) bovine serum albumin (BSA)-containing phosphate saline buffer (PBS) supplemented with 10% Normal goat serum and 0.1% (v/v) Triton X-100. This was followed by 30-min incubation in 5% BSA in PBS containing 0.1% (v/v) Triton X-100 and primary antibodies, three times 10-min washing in PBS, 30-min incubation in 5% BSA in PBS containing 0.1% (v/v) Triton X-100 and secondary antibodies, and three times 10-min washing in PBS. Appropriate excitation and emission bandpass filters were used for imaging the labeled neurons.

Image analysis

Time-lapse images were loaded in MATLAB (Mathworks, Natick, MA) and after de-noising and high pass temporal filtering, active synapses were detected as local maxima on the first derivative over time of the image stack. Regions of interest (ROIs) from which fluorescence was to be sampled were defined by dilating the maxima to a disk of radius 4 pixels (700 nm). Taking the first derivative over time allowed us to more clearly resolve fluorescence changes associated with evoked or spontaneous release and localize release sites. The differential filter also corrected slow fluctuations and drift in raw fluorescence allowing for automated threshold based event detection over minutes long image acquisitions.

Release probability calculation

To characterize the release properties of individual synapses, filtered fluorescence traces were used for peak detection. Peaks with the amplitude seven times greater than standard deviation of baseline trace during spontaneous imaging were counted as a successful glutamate release event (Fig. S2). Spontaneous frequency was calculated from the total number of events detected during 5-min

acquisition. Evoked probability for each synapse was obtained by dividing the number of events happening within one frame after stimulation by the total number of stimulation.

Quantal release analysis

To measure the quantal amplitude of evoked glutamate release, we performed 5-min continuous evoked imaging at 20 Hz while applying field stimuli at 0.5 Hz. Active ROIs were detected as described above. Florescence traces of individual ROIs were extracted from the raw image. Next, $\Delta F/F_0$ at all stimuli loci were calculated as the difference between the averaged value of 10 to 4 frames preceding and the three frames spanning the stimuli, divided by background subtracted baseline. Normalized evoke-release amplitudes ($\Delta F/F_0$) were then fit to an Expectation-Maximization (EM) Gaussian Mixture Model (McLachlan 2000). Maximum likelihood estimation was used to determine the best fit for the model for a given number of components. Because the likelihood of a fit increases with the number of free parameters, the quality of models with different numbers of fitted components was evaluated using Akaike information criterion (AIC) (Akaike 1973) in order to balance the goodness of fit with the model complexity. Models with a minimal AIC were selected as the preferred gaussian mixture model.

Sub-pixel localization analysis

Localization analysis was performed by custom-written scripts in MATLAB and Fiji. Briefly, in order to characterize the spatial organization of spontaneous and evoked glutamate release events in a single synapse, we chose synapses with at least 10 evoked responses and at least 5 spontaneous release events (182 synapses in total). The acquired signal of all recorded release events were baseline-subtracted and to estimate the molecular position of the fluorescent emitters their recorded point-spread functions were fitted a 2D Gaussian distribution by a least squares fitting (based on Levenberg-Marquardt algorithm) (Ovesny, Krizek et al. 2014). The resulting list of sub-pixel coordinates ("localizations") were loosely filtered for localization uncertainty (< 150 nm) and standard deviation (σ < 2.5 µm) to remove outliers.

Equal sample sizes of randomly picked localizations from evoked or spontaneous emission events were selected and the distances between all possible neighbors were calculated. The farthest distances from ten different subsets of the same synapse were averaged. These farthest values for each transmission mode of 182 synapses were plotted in a cumulative histogram. The density of spontaneous events occurring in evoked release areas and inside spontaneous release areas were calculated as the number of events divided by the respective areas for each synapse, measured as the 2D convex hull of their respective sub-pixel coordinates.

Spatial correlation analysis

The distances between all pairs of synapses in a given measurement were computed. Pairs of synapses were grouped by their mutual distance between 0 to 45 µm into 2.2 µm bins. For each bin of synapse pairs, the Pearson Correlation Coefficient (PCC) of evoked probability, spontaneous frequency, or flat-field corrected Bassoon intensities were computed. PCC was then plotted as a function of distance and fitted with an exponential to determine the correlation length constant. As shown in Fig. S5A-B, no correlation was observed for randomly generated dataset (blue circles).

Determination of relative protein abundance at single synapses

Image stacks of functional recording together with antibody-labeled images were loaded in MATLAB, and after drift correction, the same analysis as described above was used for ROI detection. The center of ROIs were then superimposed on antibody-labeled images and the integrated intensities were collected form flat-field corrected antibody-labeled images. We then obtained the relative abundance of all the proteins by normalizing the integrated intensity of the protein of interest by the integrated intensity of Bassoon at the same ROI. ROIs with relative protein abundance greater than 1.5 × interquartile range above the third quartile were defined as outliers and removed from further analysis.

To obtain the relative enrichment of tested proteins in spontaneous synapses, the relative abundance of proteins in spontaneous synapses was divided by their corresponding relative abundance in evoking synapses of the same cell.

Normalization of Bassoon intensities

To pool the data from all cells, the flat-field corrected Bassoon intensities of synapses in each cell were normalized to that of synapses of the cell with low evoked probabilities (< 0.1) and low spontaneous frequencies (< 0.005). The normalized Bassoon intensities together with the evoked probabilities and spontaneous frequencies of synapses were compiled from all the cells. To plot the functional properties of the synapses versus their size, the data were binned based on normalized Bassoon intensities and the averaged evoked probabilities and spontaneous frequencies per bin were calculated.

Statistical analysis

Differences between the farthest distance distributions for evoked and spontaneous release were evaluated with the Kolmogorov-Smirnov test (n = 182 synapses).

To cancel out the variation in immune-labeling efficiency between replicates, direct comparisons between the relative abundance of proteins in spontaneous and evoking synapses of the same cell were performed. Statistical significance of differences was evaluated using 2-sided Student's *t*-tests for paired samples.

Pearson's χ^2 test was used to compare the distribution of the number of captured spontaneous events over 5 minutes with the expected number of events assuming a Poisson distribution.

Supplementary Table S1. Antibodies used for immuno-labeling, related to Figure 5.

Antibody	RRID	#Catalog	Company
Bassoon	AB_2290619	141 004	Synaptic Systems
Vti1a	AB_2619865	165 003	Synaptic Systems
VAMP7	AB_2212953	232 003	Synaptic Systems
Syntaxin 12/13	AB_2198238	110 131	Synaptic Systems
VAMP4	AB_887816	136 002	Synaptic Systems
VAMP2	AB_887811	104 211	Synaptic Systems
Synapsin 1	AB_11042000	106 103	Synaptic Systems
Synaptotagmin7	AB_887838	105 173	Synaptic Systems
Doc2b	AB_2619874	174 103	Synaptic Systems
Synaptotagmin1	AB_887832	105 011	Synaptic Systems
Munc18-1	AB_2196686	116 011	Synaptic Systems
Complexin 1/2	AB_2619793	122 003	Synaptic Systems
Munc13-1	AB_887733	126103	Synaptic Systems
CF-680 anti-rabbit IgG H+L		SAB4600200	Sigma-Aldrich Chemie GmbH
Alexa Fluor 488 anti-rabbit IgG H+L	AB_2338052	111 545 144	Jackson ImmunoResearch
Cy5 anti-mouse IgG H+L	AB_2338714	115 175 166	Jackson ImmunoResearch

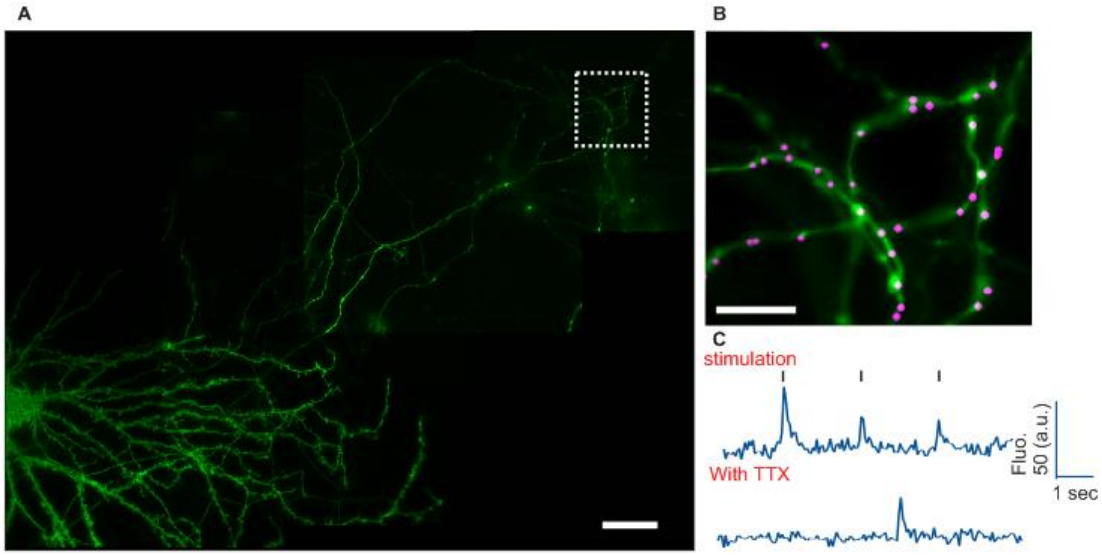

Fig. S1. Detection of glutamate release at axonal terminals, related to Figure 1. (**A**) Sparse expression of iGluSnFR was achieved by chemical transfection of cultured neurons at 4-7 DIV. Evoked and spontaneous glutamate release imaging was performed at the axonal projections of an iGluSnFR-expressing cell. (**B**) Magenta spots represent areas where glutamate release activities were detected. (**C**) Examples of raw fluorescence traces from individual presynaptic boutons upon 0.5 Hz stimulation (top) and during TTX incubation. Scale bars are 40 μm in (**A**) and 10 μm in (**B**).

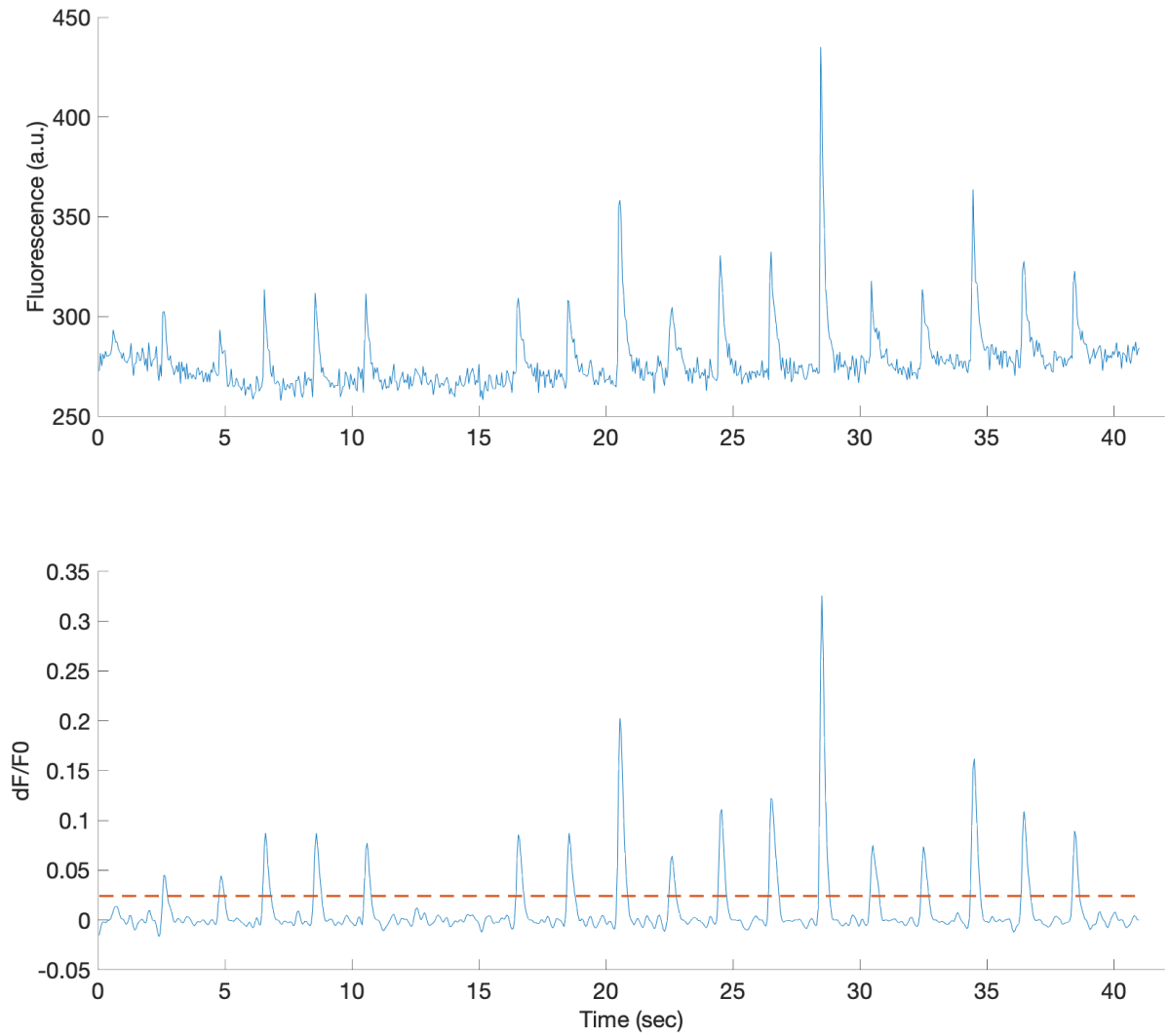

Fig. S2. Detection of successful glutamate release events in individual fluorescence traces, related to Figure 1. Representative raw fluorescence trace (upper graph) as well as its first derivative (bottom graph) recorded from a single synapse in response to 20 electrical stimuli. Dashed line in the bottom graph represent the threshold which was used to define successful release events. Peaks with amplitudes greater than this threshold were counted as a successful glutamate release event

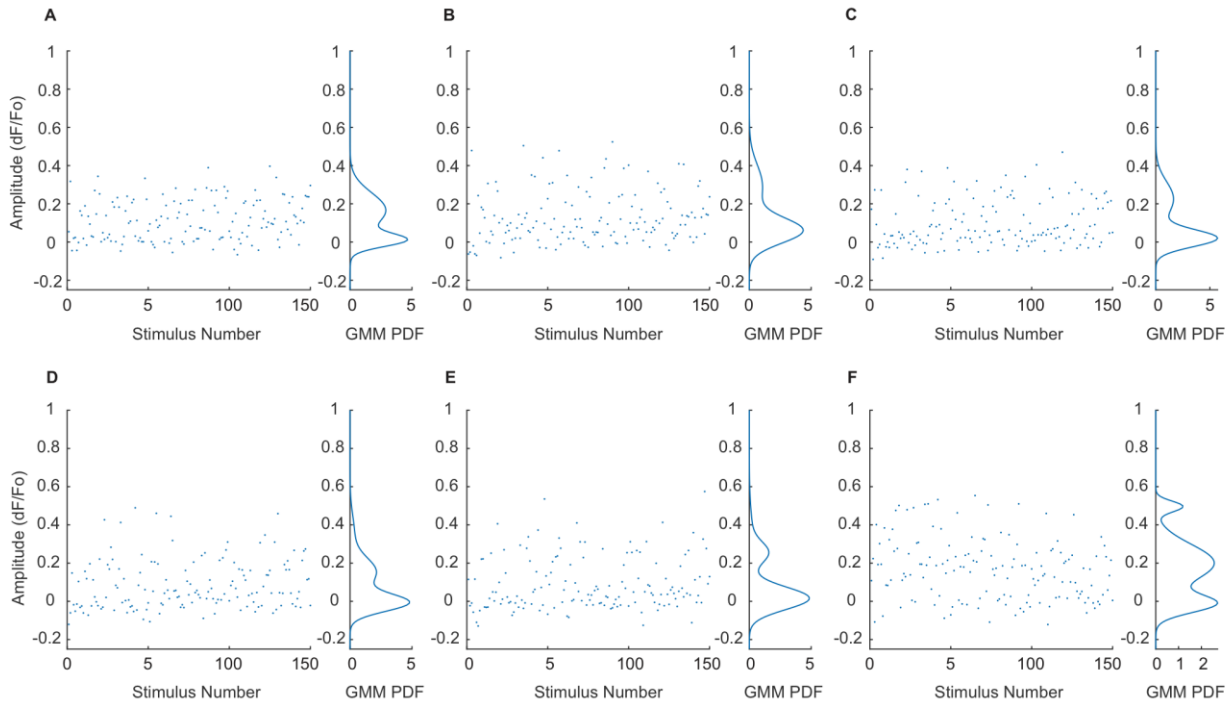

Fig. S3. Quantal analysis of glutamate release at single synapses, related to Figure 2. Fluorescence change magnitudes associated with electrical stimulations were fit for individual synapses with an Expectation Maximization Gaussian Mixture Model. The peaks around zero represent release failures, and the subsequent peaks represent the unitary (A-C) and multi-quantal release (D-F).

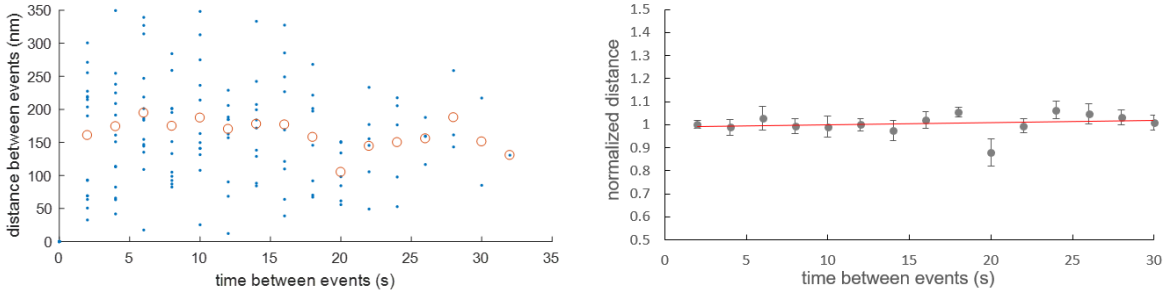

Fig. S4. The distance between release event localizations does not depend on the inter-release interval, related to Figure 3. A) The blue points represent distance between all pairs of release events in a single synapse during 20 AP stimulus train at 0.5 Hz plotted as a function of the time interval between the pair of events. The open red circles represent the mean distance between all pairs of events for a given separation time interval. B) The average of mean normalized localization distance for pairs of release events from 6 synapses are plotted as a function of the time between release events. The mean distance shows no apparent correlation with inter-release interval (Pearson correlation coefficient = 0.20) and a linear fit to the data shows negligible slope (slope = 0.001, R^2 = 0.041).

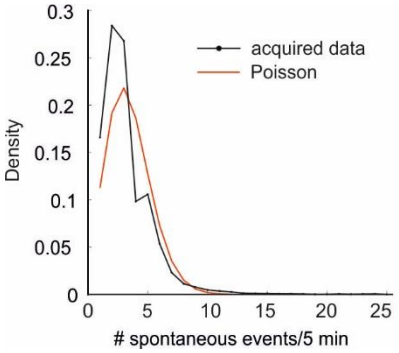

Fig. S5. Non-Poisson distribution of spontaneous events, related to Figure 4. The number of captured spontaneous events over 5-min image acquisition was pooled from more than 24,000 synapses and binned into a histogram (black distribution). The histogram does not fit well with a single Poisson distribution (red fit) ($p < 0.00001$, χ^2 test).

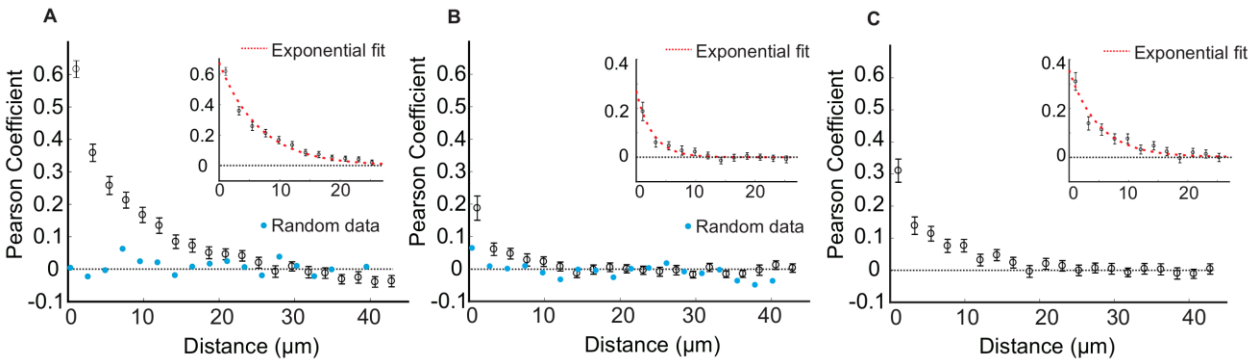

Fig. S6. Spatial correlation of release properties and synaptic size among neighboring boutons, related to Figure 4. The mean ± SEM of spatial correlation coefficients (n = 61 cells) for evoked probability (**A**), spontaneous frequencies (**B**), and Bassoon flat-field corrected intensities (**C**) was plotted for synapses up to 45 μm apart. Blue circles represent the same analysis on random generated synapse locations with random evoked probabilities (**A**) and spontaneous frequencies (**B**), indicating that the observed spatial correlation in empirical data is significant. Insets: single exponential fits to the initial 25 μm results in a length constant of 6.7 μm (95% confidence interval: 5.8, 8.3) in (**A**), 2.7 μm (95% confidence interval: 2.12, 3.8) in (**B**), and 5.0 μm (95% confidence interval: 3.9, 6.8) in (**C**).

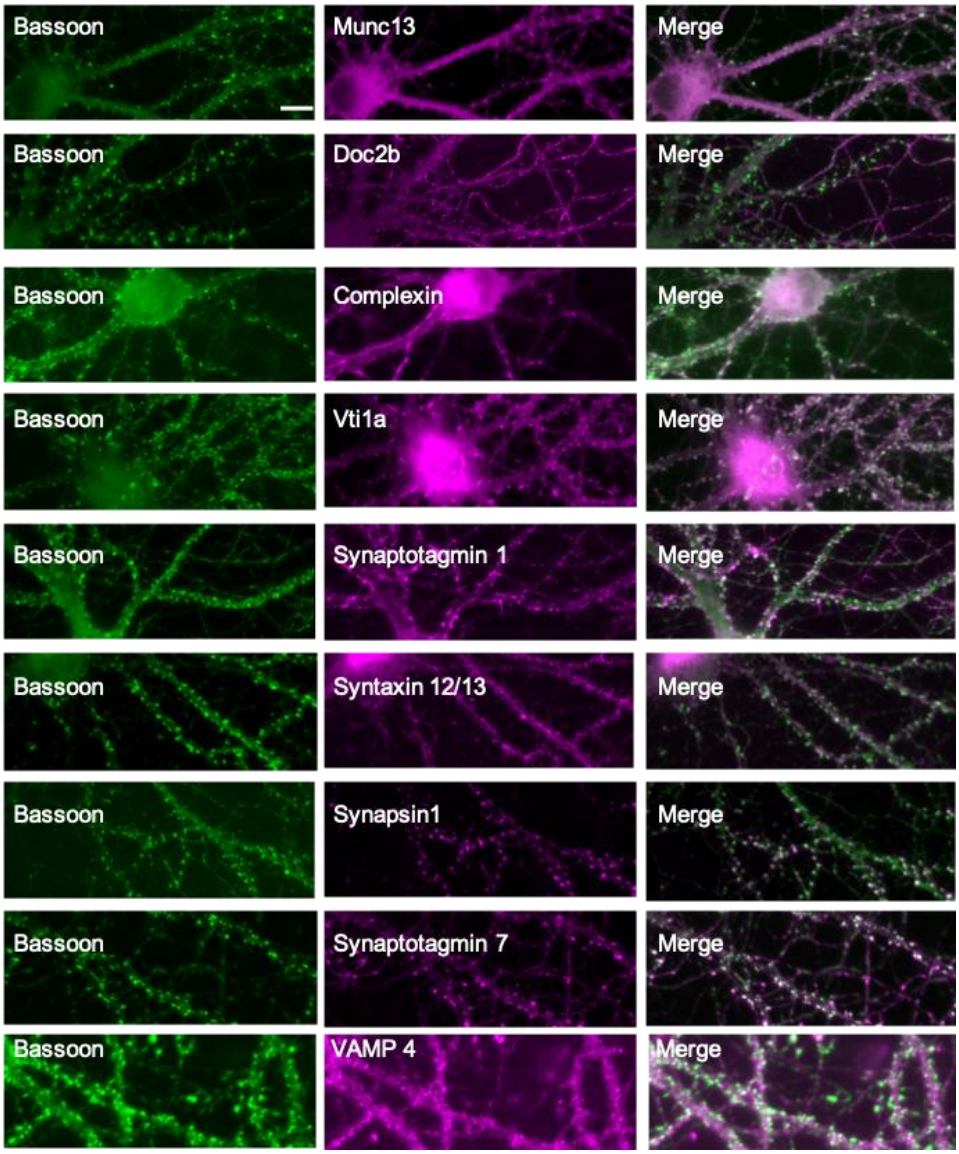

Fig. S7. Expression profile of different proteins at hippocampal synapses, related to Figure 5. Immuno-labeling against Bassoon and different proteins of interest was performed to check for the variability of their relative expression among central synapses. Scale bar 10 µm.

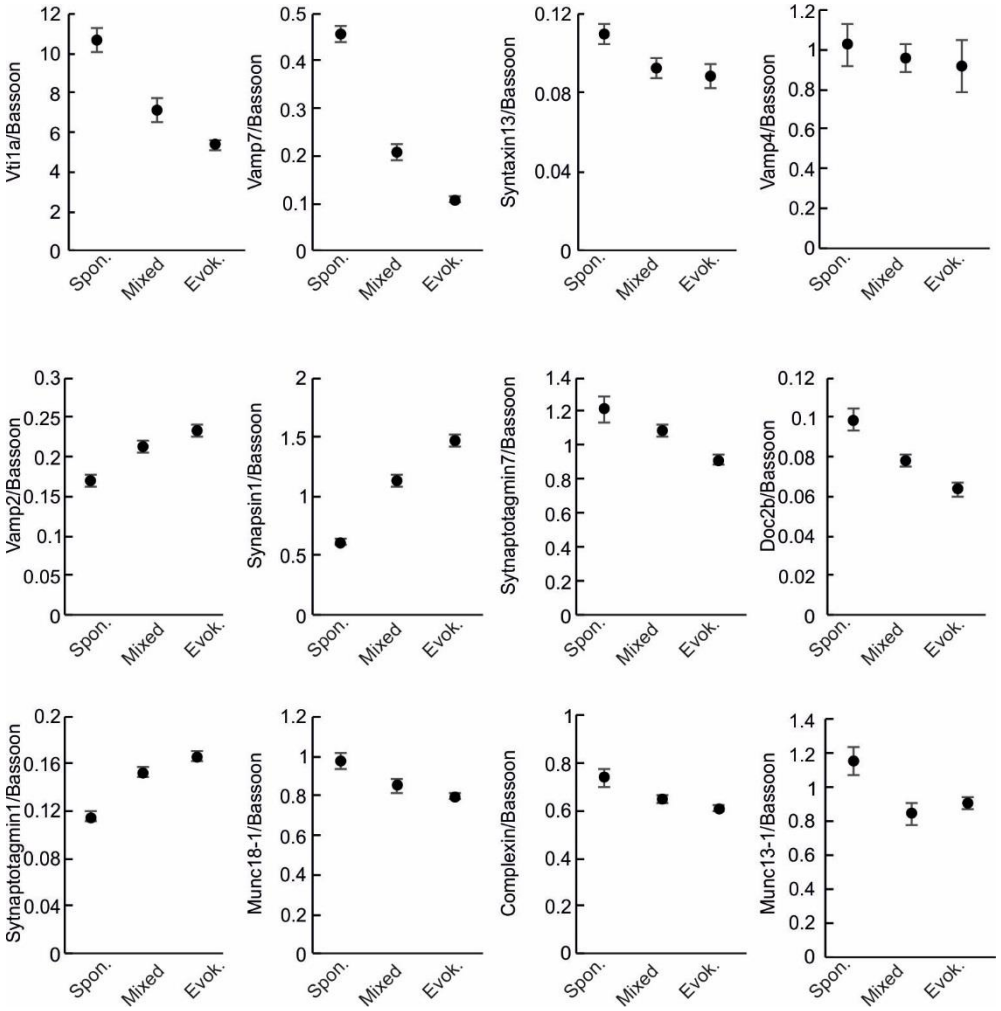

Fig. S8. Relative abundance of proteins in different pools, related to Figure 6. The relative abundance of tested proteins in the 'Mixed' pool was found to be in between the measured abundance in 'spontaneous' and 'evoking' pools. Each graph is from an example cell labeled with the indicated protein. Error bars indicate SEM (n > 50 synapses).

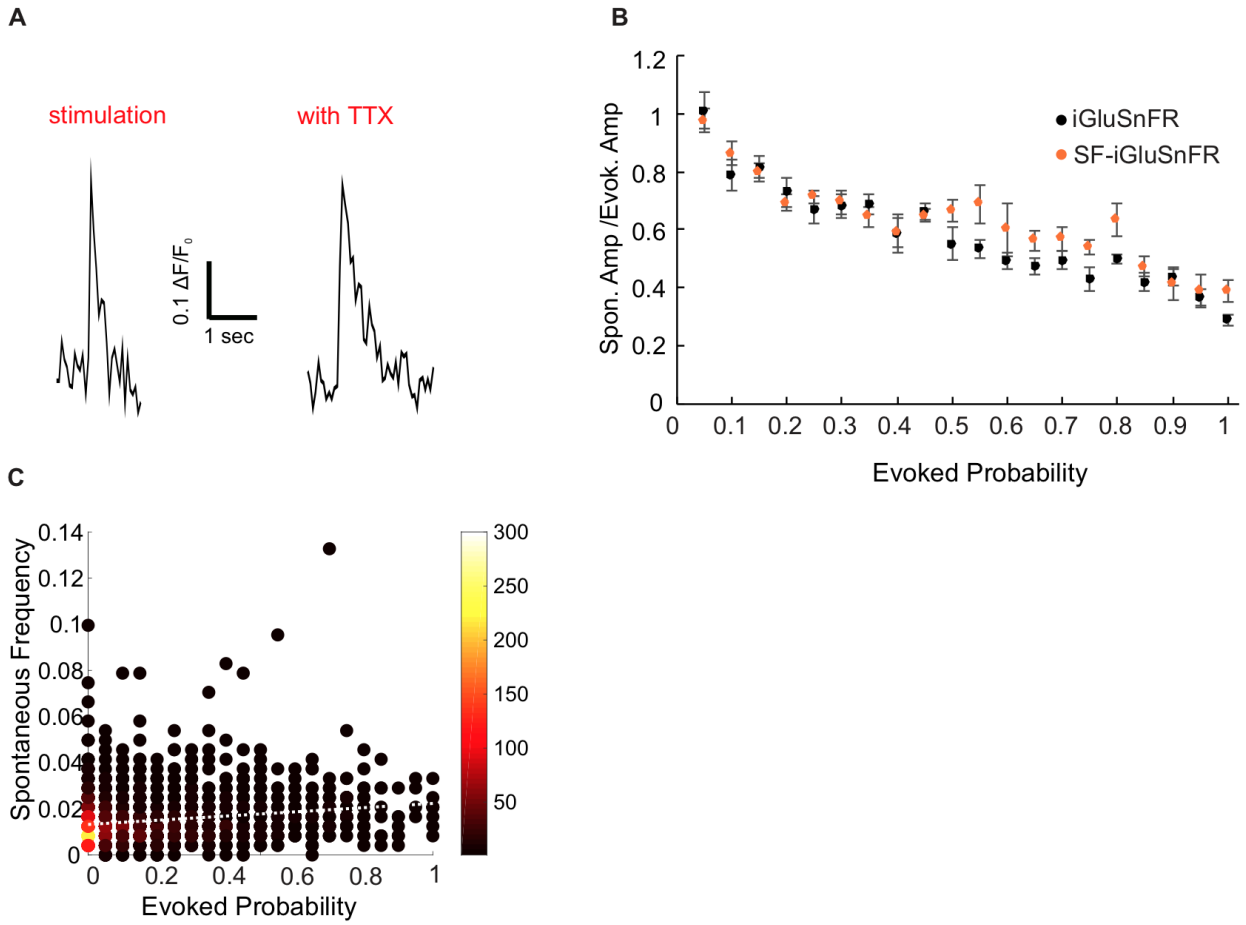

Fig. S9. Characterization of release properties with SF-iGluSnFR, related to figure 2. SF-iGluSnFR is a variant of iGluSnFR in which the circularly permutated eGFP is replaced with circularly permutated superfold (SF) GFP. This variant is reported to improve the *in vivo* imaging of stimulus-evoked glutamate release in comparison with iGluSnFR (Marvin, Scholl et al. 2018). We were able to obtain the same results by repeating the key experiments of our study with SF-iGluSnFR. (**A**) SF-iGluSNFR fluorescence change in response to stimulus-evoked and spontaneous glutamate release (in the presence of TTX) show similar amplitudes. (**B**) Similar to iGluSnFR results, a decrease in ratio of spontaneous amplitude (acquired during the first minute)/evoking amplitude at synapses with higher evoked probabilities was observed, which indicates a higher likelihood of multi-quantal release at these synapses. (**C**) No correlation was observed between the evoked release probabilities and spontaneous frequencies calculated from the measurements with SF-iGluSnFR (R^2 = 0.03), suggesting that these release modes do not share a common mechanism.

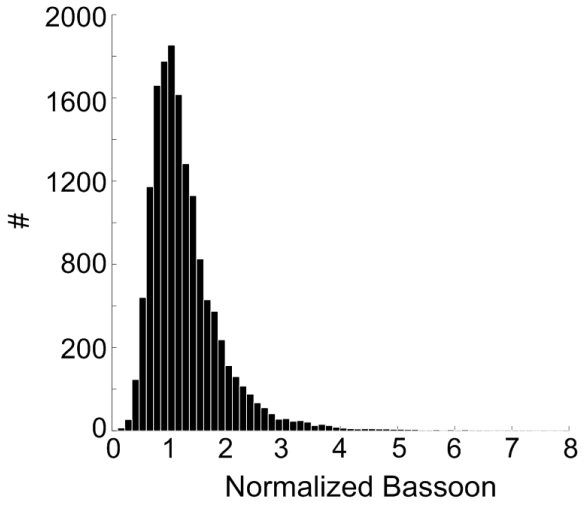

Fig. S10. Distribution of Bassoon intensities, related to Figure 6. In order to compile the Bassoon intensities from all the cells, the flat-filed corrected Bassoon intensities in each cell were normalized to the averaged Bassoon values collected from the synapses of the same cell with low evoked probabilities (< 0.1) and low spontaneous frequencies (< 0.005). The normalized Bassoon values were then pooled and binned into a histogram. An averaged value of 1.3 ± 0.73 (SD) was obtained from the total of ~ 15000 synapses (n > 60 cells).